UF-CRDS: A PULSED UNIFORM SUPERSONIC FLOW APPARATUS COUPLED WITH CONTINUOUS-WAVE CAVITY RINGDOWN SPECTROSCOPY

A Dissertation presented to

the Doctoral Committee of Shameemah Thawoos

at the University of Missouri Columbia

Department of Chemistry

_____

In Partial Fulfillment

of the Requirements for the Degree

Doctor of Philosophy

_____

by

Shameemah Thawoos

Prof. Arthur G. Suits, Dissertation Supervisor

May 2022

The undersigned, appointed by the dean of the Graduate School, have examined the dissertation entitled
UF-CRDS: A PULSED UNIFORM SUPERSONIC FLOW APPARATUS
COUPLED WITH CONTINUOUS-WAVE CAVITY RINGDOWN
SPECTROSCOPY

presented by _Shameemah Thawoos_,

a candidate for the degree of _PhD in Chemistry,

and hereby certify that, in their opinion, it is worthy of acceptance.

_____

Professor Arthur G Suits

_____

Professor Michael Greenlief

_____

Professor Justin Walensky

_____

Professor Gavin King

This dissertation is dedicated to my mother whose love, encouragement and prayers of day and night made my journey a success and to my husband whose love and support made all these possible.

ACKNOWLEDGEMENTS

TABLE OF CONTENTS

LIST OF FIGURES

reaction. Adopted with permission from Suas-David, N.; Thawoos, S.; Suits, A. G., A uniform flow–cavity ring-down spectrometer (UF-CRDS): A new setup for spectroscopy and kinetics at low temperature. The Journal of Chemical Physics **2019,** 151 (24), 244202.

characterizations is only lowered by the diameter of the isentropic core from pitot measurement which is shrinking with the distance. Indeed, contrary to our simulation, the stagnation conditions are not held indefinitely leading to a shorter flow. (B) Evolution of several indicated thermodynamic parameters along the flow axis measured by a pitot probe. Adopted with permission from Suas-David, N.; Thawoos, S.; Suits, A. G., A uniform flow–cavity ring-down spectrometer (UF-CRDS): A new setup for spectroscopy and kinetics at low temperature. The Journal of Chemical Physics **2019,** 151 (24), 244202.

LIST TABLES

ABBREVIATIONS

cw-CRDS Continuous wave cavity ringdown spectroscopy

CRESU "*Cinétique de Réaction en Ecoulement Supersonique Uniforme*"

     (translates to "reaction kinetics in uniform flow)

LIF   Laser induced fluorescence

UF-CRDS Uniform flow-cavity ringdown spectroscopy

CPUF   Chirped pulse Fourier-transformed mmWave spectroscopy with

     uniform flow

SKaR   Simultaneous kinetics and ringdown

AOM   Acoustic optical modulator

PZT   Piezoelectric transducer

ECDL   External cavity diode laser

DFB   Distributed feedback diode laser

FSR   Free spectral range

CFD   Computational fluid dynamics

PLA   Poly lactic acid

PREFACE

This dissertation is based on the newly build apparatus which couples continuous wave cavity ringdown spectroscopy and the pulsed Laval flow. The majority of chapter 3 presented here is from the published work, (Suas-David, N.; Thawoos, S.; Suits, A. G., A uniform flow–cavity ring-down spectrometer (UF-CRDS): A new setup for spectroscopy and kinetics at low temperature. The Journal of Chemical Physics 2019, 151 (24), 244202.) and the apparatus design was pioneered by former post-doctoral fellow Dr Nicolas Suas-David with whom I closely collaborated in initial instrument design and the initial reaction kinetics described in Chapter 3.

The detailed studies presented in chapter 4 and chapter 5 are nearing completion and will be submitted soon.

ABSTRACT

Investigating low temperature reaction kinetics of elementary reactions is key to understanding many phenomena of astrochemical importance. Since the introduction of CRESU (*A French acronym that stands for reactions kinetics in uniform supersonic flow)* method it has been widely used to study many reactions at temperatures as low as 13 K. The uniform supersonic flow provides a continuous flow with unform temperature and density which act as a wall-less configuration avoiding condensations effects along the walls when cooling down to low temperatures. The uniform flow is achieved by a Laval nozzle (a convergent-divergent nozzle). Traditionally, laser induced fluorescence (LIF) is used to probe reactants in the flow.

In this thesis I describe a new instrument in which highly sensitive continuous wave-cavity ringdown spectroscopy (*cw*-CRDS) is coupled with a pulsed uniform flow for the first time, a "uniform flow cavity ringdown spectrometer," UF-CRDS. The UF-CRDS setup is equipped with a pulsed uniform flow system which is produced by means of a high throughput piezoelectric stack valve combined with a Laval nozzle. In addition to the Laval nozzles built in collaboration with Dr. I.R. Sims from University of Renne, 3D printed Laval nozzles designed using a Matlab program developed in-house are also used. These nozzles are validated experimentally as well as theoretically using a computational fluid dynamics program, OpenFOAM.

Cavity ringdown spectroscopy is an absorption technique which measures the rate of decay of trapped light with an optical cavity made by two

high reflectivity mirrors. As this method measures the rate of decay of light instead of light intensity, it is largely immune the intensity fluctuations of the light source. The UF-CRDS apparatus is equipped with a DFB diode laser or an ECDL laser that can be tuned between 1411-1419 nm and 1280-1380 nm respectively. The CRDS system consists of two planoconcave high reflectivity mirrors (>99.99%) at these wavelengths. These are separated by 800 mm and with them we could achieve a maximum ringdown decay time constant of about 160 μs. For time-independent absorbing samples, the enhanced rate of power loss compared to the empty cavity leads to faster exponential decays. When the concentration of the absorbing species changes on the time scale of the empty cavity ring-down time, non-exponential decays result, for which the instantaneous decay rate in excess of the empty cavity reference case provides a time-resolved measure of the sample absorbance. S. Brown et al. recently introduced a method, simultaneous kinetics and ringdown (SKaR), where a single background normalized ringdown is applied to follow the rate of the reaction. We successfully combined the unform flow with the SKaR technique for the first time.

We choose vibrationally excited CN formed by photolysis of cyanogen bromide (BrCN) using an excimer laser operated at 248 nm (70 mJ/pulse) as our primary radical species of interest. This molecule has relatively strong transitions in the frequency range of the DFB laser and is a highly reactive radical so it makes an excellent candidate to demonstrate the capabilities of the instrument. We have performed detailed examination of the rate of reaction of

vibrationally excited CN(v=1) with O$_2$, NO and butadiene isomers at temperatures 70 K and 24 K.

The reaction of CN(v=1) + O$_2$ proceeds via association of the reactants to form a [NCOO] complex which then mainly follows through a lowest energy pathway leading to elimination of an O atom instead of re-dissociation or reaction to NO + CO. On the other hand, for the reaction of CN(v=1) + NO mainly follows through a pathway which leads to dissociation of the complex [NCNO], where it leads to vibrational relaxation of CN through a barrierless pathway. We have measured the rates for these reactions at both 24 and 70 K temperatures and they are in line with the experimental and theoretical calculations found in literature.

Another reaction of interest is the reaction of CN(v=1) with butadiene isomers. Both experimental and theoretical evidence suggests the isomers 1,2 and 1,3-butadiene enters through a barrierless PES to form long lived C$_5$H$_6$N complexes. We have measured the rate of reaction for both reactions and we see a substantial difference in their reaction rate. The rate of reaction for the 1,3-butadiene is in excellent agreement with the reported rates for the reaction with (v=0), suggesting no evidence of vibrational enhancement. The related reaction of CN with 1,2-butadiene at low temperatures has not been studied, to our knowledge.

.

CHAPTER 1

INTRODUCTION

1.1 Introduction

In this dissertation we present a new apparatus, UF-CRDS (Uniform Flow Cavity Ringdown Spectroscopy) which provides an additional avenue to study reactions at temperatures as low as 15 K with improved sensitivity and resolution. UF-CRDS combines continuous wave cavity ringdown spectroscopy (*cw*-CRDS) with a pulsed uniform supersonic flow to study elementary reactions that could give insight into chemistry in astrophysical environments such as molecular clouds and planetary atmospheres. Studying reaction kinetics in uniform supersonic flows, or the CRESU[4] technique (French acronym: *Cinétique de Réaction en Ecoulement Supersonique Uniforme*) provides a unique advantage of a "wall-less" reactor where condensation due to the low temperature is largely avoided enabling a range of studies of reactions at very low temperatures. The pulsed uniform flow system implemented in UF-CRDS minimizes the pumping requirements and gas consumption compared to the traditional continuous flow[5,6]. Moreover, the traditional probing method used in a CRESU apparatus has been laser induced florescence (LIF). UF-CRDS successfully implements near infrared continuous wave cavity ringdown spectroscopy instead. Cavity ringdown spectroscopy (CRDS) is a sensitive absorption technique that involves measurement of the rate of decay of light in a cavity caused by an absorbing species rather than measuring the absolute

intensity of light propagating through. The major advantage over LIF is that CRDS is immune to the source laser fluctuations which can be major contributor to the uncertainty of the final measurement. The first instrumentation using CRDS as a spectroscopic tool was pioneered by O'Keefe A. et al. in 1988 using a pulsed laser source[7]. Since then, instrumentation has been developed to achieve high sensitivity spectroscopic data and adopted for several different experimental conditions. The UF-CRDS experiment here adopts a continuous wave laser source, as first described by Romanini D. et al. in 1997[8].

This thesis presents the development of the instrument and demonstrates its performance in spectroscopic characterization of the uniform flow and in low temperature kinetics measurements. For the latter, reactions of CN(v=1) with multiple co-reactants have been studied from 15 to 70K using this apparatus. The rates of reactions are measured using a method first described by Brown S.S. et.al[9] referred to as SKaR (Simultaneous Kinetics and Ringdown). This method takes advantage of the long hydrodynamic time in the flows to monitor reactions that occur within the same time scale as the ringdown decay of the optical cavity.

1.2   Basics of optical cavities

In an optical cavity or an optical resonator light is trapped between an arrangement of reflective surfaces allowing an increased path length. In a standard CRDS the commonly used optical cavity is made of two parallel highly reflective mirrors where at least one of them is a concave mirror. The following

concepts associated with optical cavities are important in understanding the CRDS implementation and reviewed briefly here.

1.2.1 Cavity Q and Finesse

Cavity Q (quality factor) is a measurement of how well an optical resonator stores the optical energy within. It is defined as,

$$Q = 2\pi \frac{Optical\ energy\ stored\ in\ the\ cavity}{Optical\ energy\ lost\ in\ one\ cycle\ of\ oscillation} \qquad (1.1)$$

A cavity that stores the energy more efficiently has a higher Q. Q also can be defined in terms of line width of the cavity resonance (Δv) and center of the resonance frequency (v_0).

$$Q = \frac{v_0}{\Delta v} \qquad (2)$$

Cavity finesse (F) is measure of the width of the cavity resonances and it is defined as,

$$F = \pi \sqrt{R}/(1 - R) \qquad (3)$$

Where R is the reflectivity of the cavity mirror. Figure 1.1 is an illustration of cavity transmission with varying mirror reflectivity[10]. The higher the reflectivity, the higher the finesse thus the narrower the cavity resonances are.

1.2.2 Free spectral range

Free spectral range (FSR) is a measurement of the spacing between two
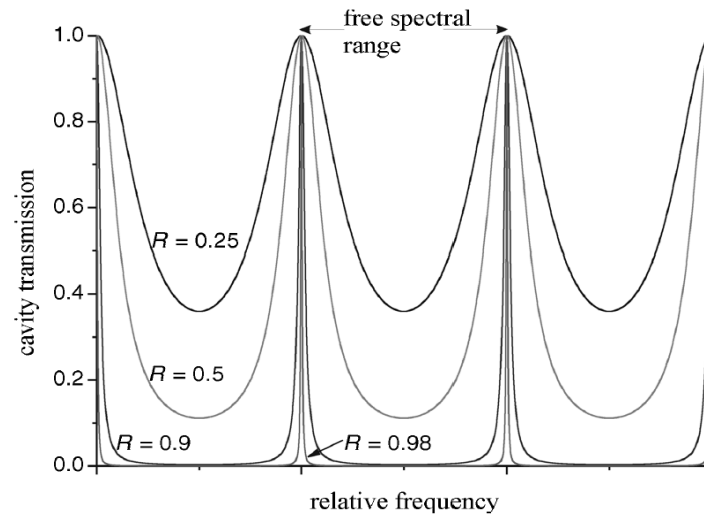
Figure 1.1. The transmission for an optical cavity with varying mirror reflectivity R. Adapted with permission from Van Helden, J.; Peverall, R.; Ritchie, G.; Berden, G.; Engeln, R., Cavity enhanced techniques using continuous wave lasers. Wiley-Blackwell West Sussex, UK: 2009.

adjacent modes in an optical cavity (Figure 1.1). It is a measurement of

frequency and can be presented as (for a longitudinal mode in a

nonconfocal geometry),

$$\delta_{FSR} = \frac{c}{2L} \qquad (4)$$

Where c is the speed of light and L is the linear cavity length.

1.2.3 Optical stability

Optical stability is a measurement of the stability of the modes in an

optical resonator. This can be defined in terms of a stability parameter,

g.

$$g_n = (1 - L/r_n) \tag{5}$$

Where r_n is the radius of curvature and the n is the mirror index. Stable resonators are produced only for a limited range of r_n. To construct a stable cavity the g parameters for the mirrors used should fulfill the following criteria[11],

$$0 < g_1g_2 < 1 \tag{6}$$

1.2.4 Cavity mode structure and mode matching

There are two types of modes, longitudinal and transverse, produced by standing wave patterns due to interferences. The frequency of such modes of a cavity with two parallel mirrors can be given as,

$$\nu_{qnm} = \frac{c}{2L}[q + \frac{2(n+m+1)}{\pi}arctan(\frac{L}{\sqrt{L(2r_n-L)}}) \tag{7}$$

where, q, m and n mode indices. Mode matching plays a key role in maximizing the power that is built up in the cavity, and TEM_{00}, the fundamental mode, is preferred in cw-CRDS methods. TEM_{00} has a Gaussian form hence the mode matching can be achieved by focusing the laser beam so that it matches the cavity waist (w_0).

$$w_0 = \sqrt{\frac{L\lambda}{\pi}}[\frac{g_1g_2(1-g_1g_2)}{(g_1+g_2-2g_1g_2)^2}]^{0.25} \tag{8}$$

The selection of optics depends on the laser source used. In some cases, a simple lens is sufficient whereas in others prior shaping of the laser beam may be required.

1.3 Cavity ringdown spectroscopy (CRDS)

CRDS is a direct absorption technique which depends on a muti-pass cavity
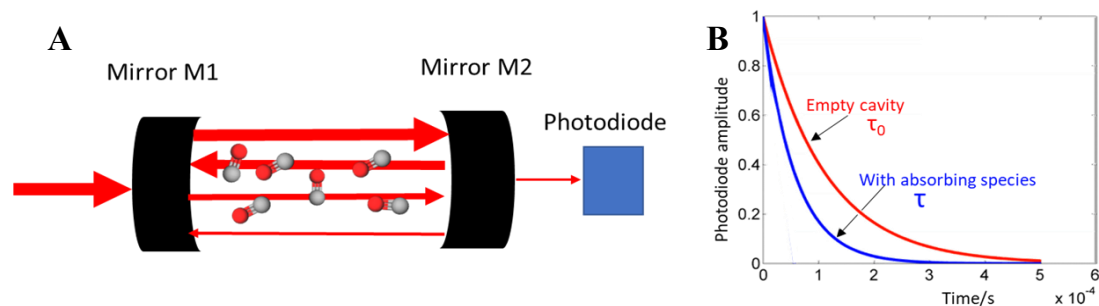
Figure 1.2. A. Schematic diagram of the CRDS cavity made of two high reflective (R>99.99%) concave mirrors. B. Schematic of cavity ringdown decay with (τ) and without (τ₀) an absorbing species in the cavity.

resulting in an extended effective path length and hence increased detection sensitivity. The instrumentation and techniques of CRDS have developed since its introduction by O'Keefe et al. in 1988[7]. In a basic CRDS setup a laser pulse is trapped between high reflectivity concave mirrors and allowed to bounce back and forth between the mirrors freely. The light transmitted through one mirror is measured with respect to time (Figure 1.2).

The transmitted light decays exponentially with time and the ringdown time (τ) is the inverse of at the rate (k) which the transmitted light decays. The rate at which the transmitted light decays depend on mirror reflectivities in the absence

of absorbing species. When some absorber is present the decay becomes faster and increases when the absorption is stronger.

$$T = (1 - R) \qquad (1)$$

$$k = (1 - R)\, {}^c/_L \qquad (2)$$

$$\tau = k^{-1} \qquad (3)$$

Where T is the transmittance, R is the reflectivity of the high reflective mirrors, c is the speed of light and L is the distance between the high reflective mirrors. However, as this cavity constructs a multi-pass cell, the effective length the light travels within the cell L_{eff} can be estimated as presented in equation (4).

$$L_{eff} = \tau c = {}^L/_{(1-R)} \qquad (4)$$

For typical conditions, where R is 99.99% , L is around 1m so L_{eff} can be on the order of 10^4. The absorption taking place can be expressed using the Beer-Lambert law,

$$I = I_0 \exp(-\alpha d) \qquad (5)$$

where I and I_0 are the transmitted and incident light intensity, d is the length of the sample, and α is the absorption coefficient of the sample. The absorption at a specific absorption peak frequency *(v)*,

$$\alpha(v) = N\sigma(v) \qquad (6)$$

7

where N is the number density and $\sigma(v)$ is the absorption cross section. The measured transmitted light intensity and the cavity parameters can be related using the Beer-Lambert law as given in equation (7) where t is the round-trip time for n number of round trips $(t_r = n \times 2L/c)$.

$$I(t) = I_0 \exp\left(- {tc}/{L} \left(1 - R + \alpha d\right)\right) \tag{7}$$

As ringdown time is the inverse rate of the transmitted light the ringdown time can be related as

$$\tau = \frac{L}{c(1+R+\alpha d)} \tag{8}$$

The ringdown time is measured by fitting the transmitted light to a least square exponential fit and the absorption spectrum of a species can be plotted by measuring the ringdown time with respect to a scan of frequencies (equation 9 and 10).

$$\tau_0 = \frac{L}{c(1+R)} \tag{9}$$

$$\frac{1}{\tau(v)} = \frac{\alpha(v)\, dc}{L} + \frac{1}{\tau_0} \tag{10}$$

1.4 Continuous wave cavity ringdown spectroscopy (*cw-*CRDS)

Pulsed lasers have been the primary choice of laser source for the CRDS experiment since its introduction by O'Keefe et al. in 1988[7]. However, pulsed lasers have limitations when it comes to high resolution CRDS. This is mostly due to the pulse-to-pulse laser fluctuations and the broader linewidth and hence excitation of multiple modes in the cavity. Multimode excitation results in multiple ringdown times which in turn contributes greatly to the uncertainty. Nearly a decade after O'Keefe, Romanini et al. introduced a configuration which incorporated a continuous wave laser source[8]. To pulse a cw laser within the cavity they introduced an acoustic optical modulator (AOM) to turn off the laser when the power builds up in the cavity reached a user-defined value. The
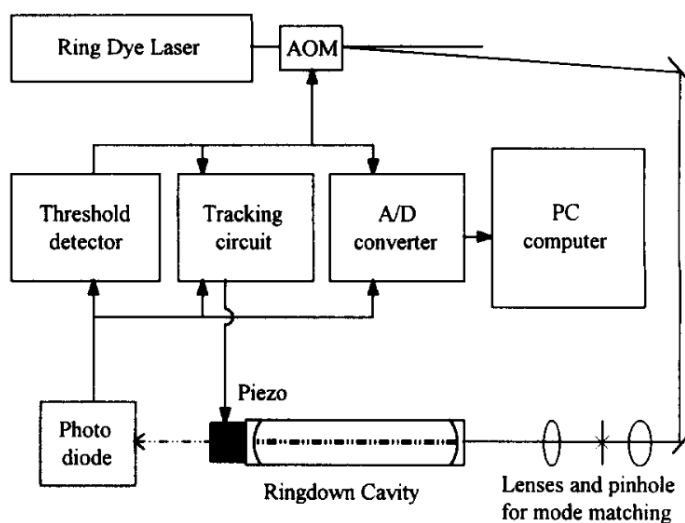
*Figure 1.3 Simplified schematic for a cw-CRDS experimental arrangement. Adapted with permission from Romanini, D.; Kachanov, A.; Sadeghi, N.; Stoeckel, F., CW cavity ring down spectroscopy. Chemical Physics Letters **1997,** 264 (3-4), 316-322.*

laser is aligned to excite the TEM00 mode of the cavity, and a photodiode

measures the transmitted light. At a predetermined photodiode intensity
threshold, the AOM is triggered to stop deflecting the light into the cavity, and
the decay of the light trapped in the cavity is observed without further power
injection. Meanwhile the photodiode measures the light transmitted and the
ringdown signal is recorded. The output mirror of the cavity is mounted on
piezoelectric transducer (PZT). As it is not possible to fix the cavity to a
precise multiple of the wavelength, the PZT is used to modulate the length of
the cavity such that the frequency of the cavity TEM_{00} mode oscillates around
the laser line. The amplitude of the PZT modulation is selected with respect to
the FSR of the cavity. Ideally it is set to less than the FSR so that only one
mode is trapped per ramp of the modulation and hence one ringdown event per
ramp of the modulation. However, the threshold for the AOM allows selection
of the lower order modes with the highest intensity, hence increasing the
sensitivity.

1.5 Reaction kinetics in uniform supersonic flow

Understanding reaction kinetics at low temperatures is key to insight into and modeling of reactions in interstellar clouds and planetary atmospheres. The temperatures in such environments can be as low as 10 K. However, traditional flow tube experiments have failed to reach temperatures below 77 K and avoiding condensation along the walls of the flow tubes has been challenge when the temperature is below 200 K. These challenges can be avoided with the CRESU technique. CRESU is a French acronym stands for "Cinétique de Réaction en Ecoulement Supersonique Uniforme" and translates to reaction kinetics in uniform supersonic flow. This method was pioneered by Rowe et al[4,12-14]. The supersonic uniform flow is produced by expanding a gas through a Laval nozzle. The Laval nozzle is convergent divergent nozzle, which was initially invented as part of a steam turbine. It is now familiar as the shape of rocket engine nozzles. The optimum Laval flow produced by this nozzle will
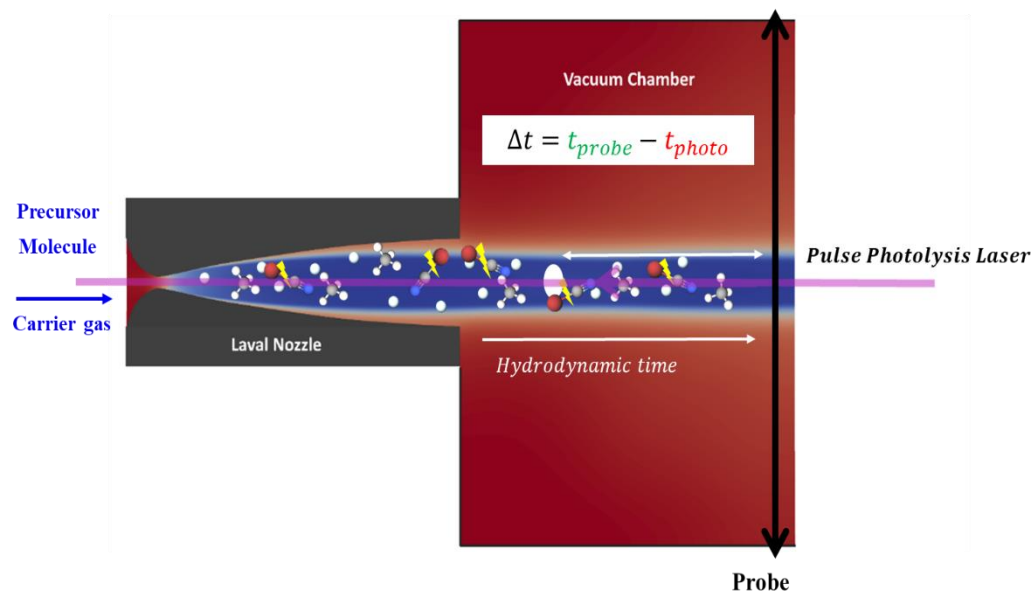
Figure 1.4 Schematic of uniform supersonic flow in a CRESU experiment.

create a "wall-less" beam with a unform flow velocity, density and temperature, which is ideal to study reaction kinetics. The profile of the Laval nozzle for a specific density, temperature condition for a given gas is unique.

In a CRESU experiment the reactants are introduced to the flow as one would normally do in a flow tube experiment. In common practice for reactions involving radicals a photolysis laser is used, often (as here) a UV excimer laser. In typical CRESU experiments the reactions are probed using laser induced fluorescence (LIF) spectroscopy[15]. LIF probes the reaction with respect to time set at a constant position with respect to the Laval nozzle exit. The arrival of the detection species at the probing region after every excimer pulse is measured. The measurement of reaction kinetics is done under pseudo-first order conditions in which the co-reactant is maintained in large excess.

1.6   Simultaneous kinetics and ringdown (SKaR)

One of the major weaknesses in implementing CRDS as a detection probe in a CRESU experiment is the finite time it requires to measure the ringdown time. Either in CRESU or in any reaction kinetics measurement method, the detection time should be negligible compared to the reaction time. However, this becomes a limitation when using CRDS as detection method in measuring reaction kinetics. In successful application of CRDS as the probing technique either reaction must be limited to slower rates or the ringdown decay ought to be faster, which limits the sensitivity of the method.

However, the long hydrodynamic time in the uniform flow is such that the ringdown and the kinetics may be on the same timescale. In this case the complete rate measurement may be achieved *in each ringdown.* This idea of measuring the ringdown and kinetics at the same time was first reported by Brown et al. in a room temperature flow. [9] They coined the term SKaR, which stands for simultaneous kinetics and ringdown. Here we describe the first implementation of SKaR in a supersonic flow, made possible by the unique conditions of the Laval expansion.

For a bimolecular reaction where,

$$A + B \rightarrow C \tag{11}$$

When [A] is in excess and change in concentration of A over the course of the reaction is considered insignificant. In such condition, *[A]$_0$ = [A]$_t$* and in such conditions the reaction is set to be pseudo-first order with respect to reactant B. To measure the rate of reaction of a reaction as such one could either monitor the loss of reactant with respect to time or formation of product. The SKaR technique could be used for either method. When applying the SKaR method it is key to note that change in transmitted light intensity I , does depend on both loss in cavity due to reflection and the change is concentration of the absorbing species along the cavity axis x. This could be related as,

$$\frac{dI}{dx} = -\alpha.\frac{L_A}{L}.I - \frac{(1-R)}{L}I \qquad] \tag{12}$$

where α is the absorbance, L is the cavity length, L_A is the length of the cavity region where the absorbing species is present and I is the transmitted light intensity. To simplify the data analysis, the SKaR method defines a ratio as in equation 13. The ratio is measured as a background normalized ringdown decay with the absorbing species.

$$Ratio = \frac{I(t)}{I_0 e^{-t/\tau_0}} = \exp\left[-c\sigma \int [A](t)dt\right] \qquad (13)$$

Where c, is speed of light, σ absorption cross section, *[A](t)* and *I(t)* is the absorber concertation and transmitted light intensity at time *t* respectively, and τ_0 is the background ringdown time which is $L/c(1-R)$.

The kinetics experiments carried out using the UF-CRDS apparatus has been implemented primarily where loss of reactant is monitored under pseudo-first order conditions. Thus, the equation 13 can be rearranged as:

$$Ratio(t) = \exp\left[-\frac{c\alpha_\infty}{k'}\left(1 - e^{-k't}\right)\right] \qquad (14)$$

where *k'* is the pseudo first order rate constant.
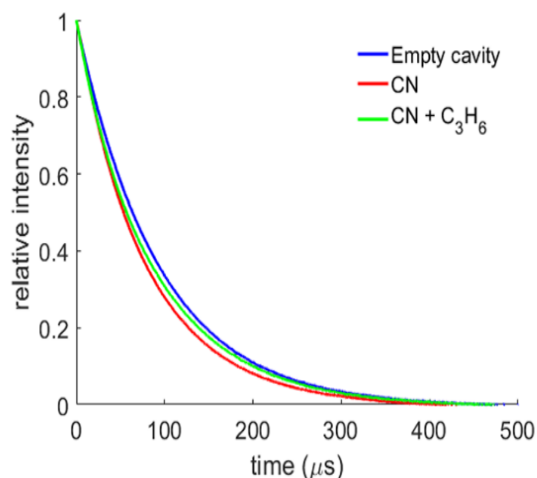
Figure 1.5 Schematic representing transmitted light at laser frequency set at a peak absorption of CN (v=1), j=5.5 with respect to time, (ringdown time decay) at three different instances. Blue trace: Empty cavity ringdown decay with no absorbing species. Red decay: Ringdown decay in the presence of CN. Green trace: the ringdown decay when co-reactant propene is added to the mixture. At earlier times the green trace follows the trace and at later times it reaches the blue trace signaling completion of the reaction. Adopted with permission from Suas-David, N.; Thawoos, S.; Suits, A. G., A uniform flow–cavity ring-down spectrometer (UF-CRDS): A new setup for spectroscopy and kinetics at

CHAPTER 2

DESIGN AND CHARACTERIZATION OF

LAVAL NOZZLES

2.1 Introduction

The Laval nozzle is a convergent divergent nozzle first introduced by Swedish engineer Gustaf De Laval for application in steam turbines. It was first widely used in modern rocket engines that use a hot gas combustion. However, in the CRESU method of studying reaction kinetics, the Laval nozzle plays a key role in creating the low temperature uniform flow. In the convergent-divergent nozzle design, the shape of the divergent part is critical in the expansion of the flow to form the uniform supersonic flow. Figure 2.1 is a schematic of the Laval nozzle.
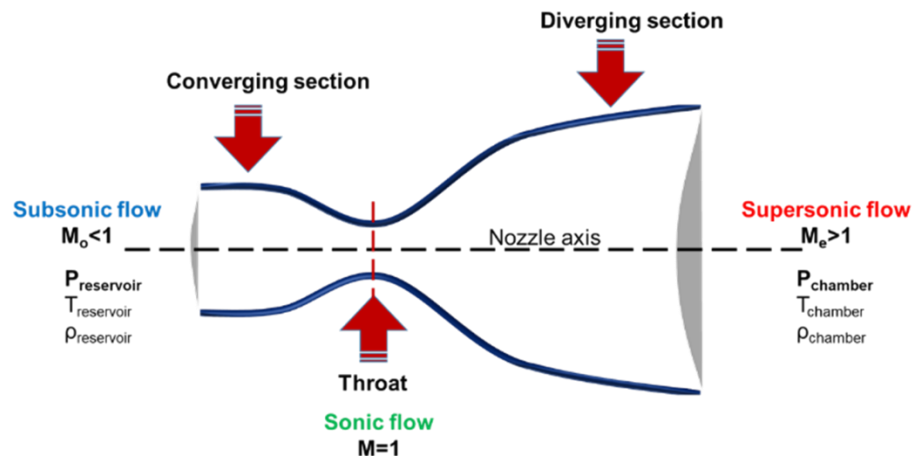
Figure 2.1 Schematic of a Laval nozzle. P is the pressure, T is temperature, ρ is the density and M is the Mach number. M_0 is the Mach at stagnation and M_e is the Mach at the exit of the nozzle.

M is the Mach number which is defined as the ratio of the flow velocity to the local speed of sound. It is a dimensionless ratio which is frequently used in fluid dynamics. Accurate design of the profile of the Laval nozzle is essential in creating a flow with the desired expansion. The methods used in calculating the nozzle profile involves two main steps[16-21]. The first involves calculating the shape responsible for the isentropic core using the "method of characteristics" while the second involves calculating the boundary layer accounting for the viscosity of the gas flow.
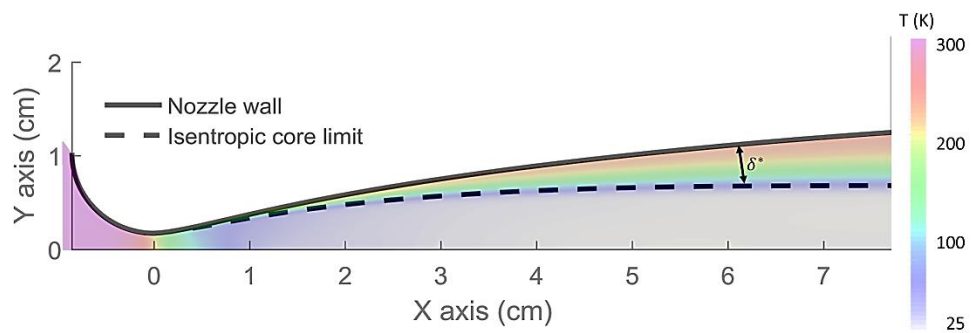
Figure 2.2 Schematic representing the isentropic core b limit and the boundary layer calculated using the home-built MATLAB program.

Most available methods to create the nozzle shape either remain inaccessible to desired flow conditions or written in outdated computer software. We have adopted the methods described by Moger, W.C. et al.[16] and Atkinson, D.B. et al[17] and use a MATLAB code with a graphical interface to design nozzles with desired flow conditions. This code was developed by Dr N. Suas-David.

The flow characterization is done experimentally using pitot mapping and validated theoretically in collaboration with Dr N. Suas-David using OpenFOAM, an open source computational fluid dynamics (CFD) program.

2.2 Fabricating Laval nozzles

One of the biggest challenges in the use of Laval nozzles is that a single nozzle only produces an ideal flow one set of conditions. This requires the use of multiple nozzles for different flow temperatures for studying reaction kinetics. Using the MATLAB program, we obtained the coordinates for the profile for the Laval nozzle (Figure 2.3)
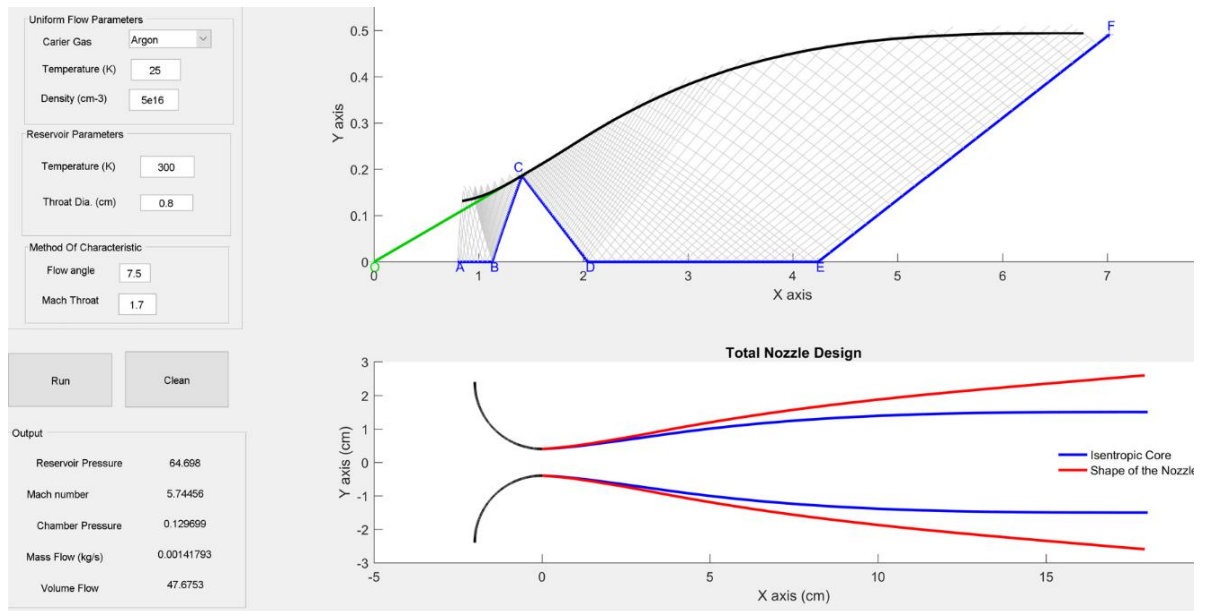
Figure 2.3 MATLAB user interface for the nozzle design program. The inputs are the carrier gas type, the temperature in K of the flow and the desired density in molecules cm^{-3}.

The coordinates generated from the MATLAB program can then be exported to a 3D modelling program such as SOLIDWORKS to create the axisymmetric three-dimensional structure, keeping the convergent-divergent profile intact. (Figure 2.4) This 3D model can then be used to fabricate the nozzle. Originally, the material of choice for the fabrication was aluminum; however, when
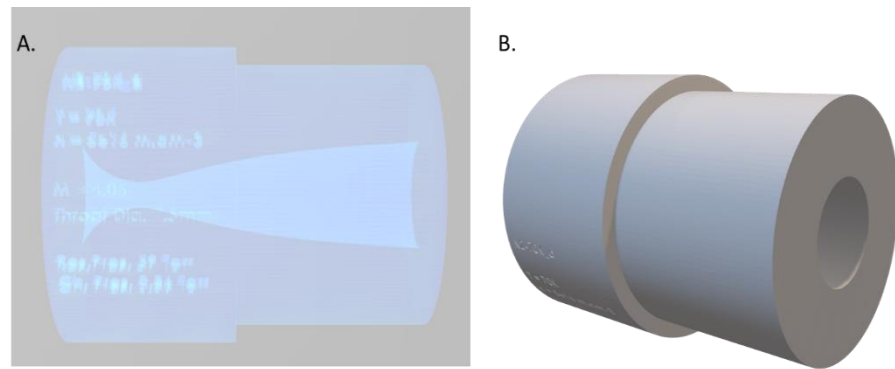
Figure 2.4 A. X-ray view, B. 3D model of the Laval nozzle created by SOLID WORKS.

developing a series of nozzles with different conditions this is costly and time consuming. We have since taken advantage of the developmental efficiency and convenience of 3D printing technology. We use a filament based commercial 3D printer (Ultimaker3-extended). The 3D model created using SOLID WORKS is exported as a gcode using the Ultimaker Cura software. We use commercially available printing PLA (Poly lactic acid) filaments. The time for the printing depends on the size of the nozzle and how dense the printing is required. Although 3D printing was initially used as an option to build test nozzles, we discovered that the PLA is a robust material that could withstand experimental conditions including exposure to the excimer laser pulses. We

now routinely use 3D printed nozzles using PLA without any post treatment of the print.

2.3 Pulsed Laval Flow

Historically, CRESU experiments used the Laval nozzles to produce a continuous uniform flow. This requires huge pumping capacities as well as gas consumption. This can be a serious drawback experimentally, financially as well as environmentally. As a solution, the pulsed Laval flow was introduced by M. Smith at Arizona[17,22,23]. The CRESU apparatus in Rennes requires a pumping

Al machined Laval Nozzle

3D printed PLA based Laval nozzles for different carrier gases Ar, He, Ne and N_2.
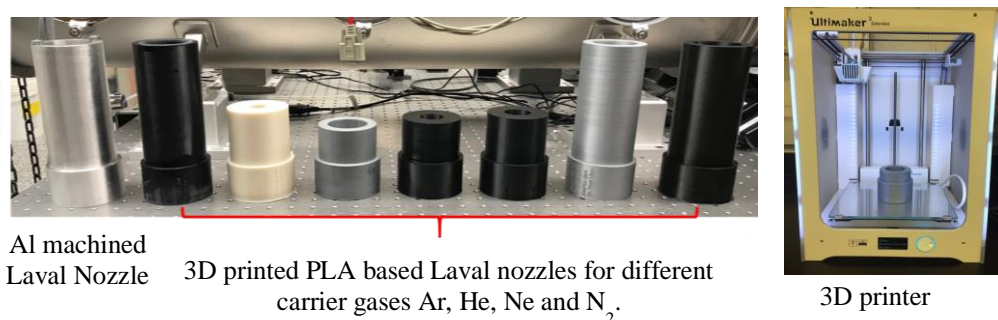
3D printer

Figure 2.5 Series of 3D printed Laval nozzles and the 3D printer used.

capacity of about 30,000 m^3h^{-1} [21] whereas the UF-CRDS achieves its highest pumping capacity from use of a single turbomolecular pump (with a pumping capacity of 8469 m^3 h^{-1}) backed by a roots dry pump (pumping capacity 100 m^3 h^{-1}).. The UF-CRDS apparatus is equipped with a pulsed Laval flow system modeled on that of the Chirped Pulsed Fourier Transformed Microwave-Uniform Flow (CPUF) apparatus developed in our group with minor modifications[5,6,24].

The pulsed Laval flow is produced by a combination of a high throughput piezoelectric stack valve[25] and a Laval nozzle. The home built high throughput piezo-electric stack valve (Physik Instrumente P216.90, 180 μm maximum travel) fills up a reservoir of about 20 cm^3. The gas flow into the piezo-electric stack valve is controlled by either one or multiple flow controllers connected to the gas cylinders. This reservoir act as a stagnation chamber prior to the expansion of the gas through the Laval nozzle. The piezoelectric stack valve is mounted parallel to the expansion but vertically shifted relative to the Laval nozzle exit ensuring the stagnation conditions. A 3 ms opening of the piezoelectric stack valve has been shown to be sufficient to rapidly fill the reservoir despite the large "leak" caused by the open nozzle throat. The pressure in the stagnation reservoir is measured using two pressure transducers, ((Kulite, XTL-190SM-0.7BARA) placed close to the input and the output of the reservoir (Figure 2.6).
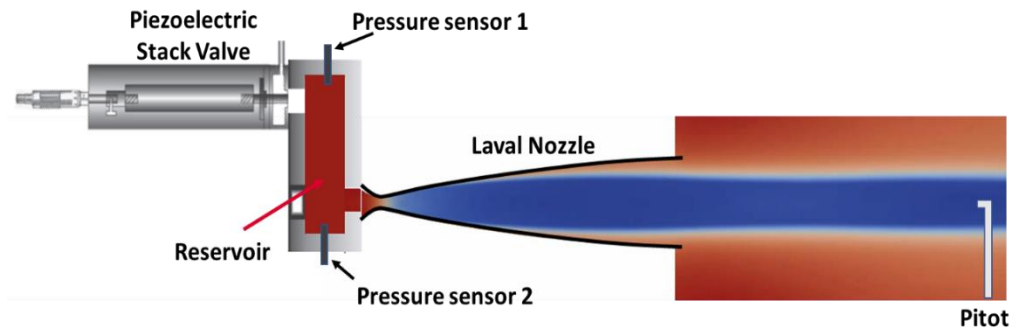
Figure 2.6 Pulsed Laval flow system. The piezoelectric stack valve, the reservoir, and the Laval nozzle.

The piezoelectric stack valve, the reservoir and the Laval nozzle are mounted on motorized actuators which allow the nozzle system to be moved vertically (IAI

- RCS2-GS5N-I-60-2.5-75-T2-S-B) [maximum translational range 60 mm] and longitudinally (IAI – RCP4-SA5C-I-42P-6-800-P3-S-B) [maximum translational range 800 mm].

2.4 Characterizing the Laval flow

To validate the flow conditions, we use a pitot probe measurement of the impact pressure of the flow. We use a pressure transducer (Kulite, either XCEL-100-0.35BARA or XTL190SM-0.7BARA) to measure the impact pressure (P_i) at various positions in the flow. The measured impact pressure can be converted to a more useful parameter, the Mach number, M using equation (2.1)

$$\frac{P_i}{P_0} = [\frac{(\gamma+1)M^2}{(\gamma-1)M^2+2}]^{\frac{\gamma}{(\gamma-1)}}[\frac{(\gamma-1)}{(2\gamma M^2-\gamma+1)}]^{\frac{1}{(\gamma-1)}} \qquad (2.1)$$

Where P_0 is the reservoir pressure and γ is the heat capacity ratio. The Mach number can be used to calculate the flow temperature and pressure using equations 2.2 and 2.3.

$$\frac{T_0}{T_f} = 1 + \frac{\gamma-1}{2}M^2 \qquad (2.2)$$

$$\frac{P_0}{P_f} = (\frac{T_0}{T_f})^{\frac{\gamma}{(1-\gamma)}} \qquad (2.3)$$

Where T_0 and P_0 are reservoir temperature and pressure respectively. And T_f and P_f are flow temperature pressure respectively. The experimental pitot measurements are compared with the CFD calculations done with OpenFOAM.

2.4.1. Impact pressure measurements

There are currently four different Laval nozzles in use in conjunction with the UF-CRDS experiments. The gases and conditions for these nozzles are listed in Table 2.1. The pitot pressure transducer is mounted on a stationary mount within the chamber whereas the nozzle assembly is mounted on a motorized actuator as described above. A LabVIEW program controls the movement of the nozzle with respect to the pitot probe and records the output of the pressure transducers both in the reservoir and the pitot probe. These Kulite sensor measurements are then used to derive the flow parameters such as temperature, pressure, and density. As the Laval nozzle could be moved both horizontally and vertically with respect to the stationary pitot probe, the impact pressure measurements could be made both axially and radially creating a 2D pitot map of the flow (Figure 2.7) The nozzle measurements were then confirmed using the CFD calculations as well as spectroscopically using CRDS which will be discussed further in Chapter 3.

Table 2.1 Summary of Laval nozzles used in UF-CRDS experiments. (P is the pressure T is temperature, and ρ is the density.)

Nozzle	Gas	Reservoir P/torr	Chamber P/torr	Flow T/K	Flow ρ/molecule cm^{-3}
N2_70K	Nitrogen	60	0.36	70	5.50×10^{16}
Ne_24K	Neon	60	0.14	24	4.50×10^{16}
He_22K	Helium	360	0.50	22	2.70×10^{17}
He_15K	Helium	90	0.05	15	3.5×10^{16}
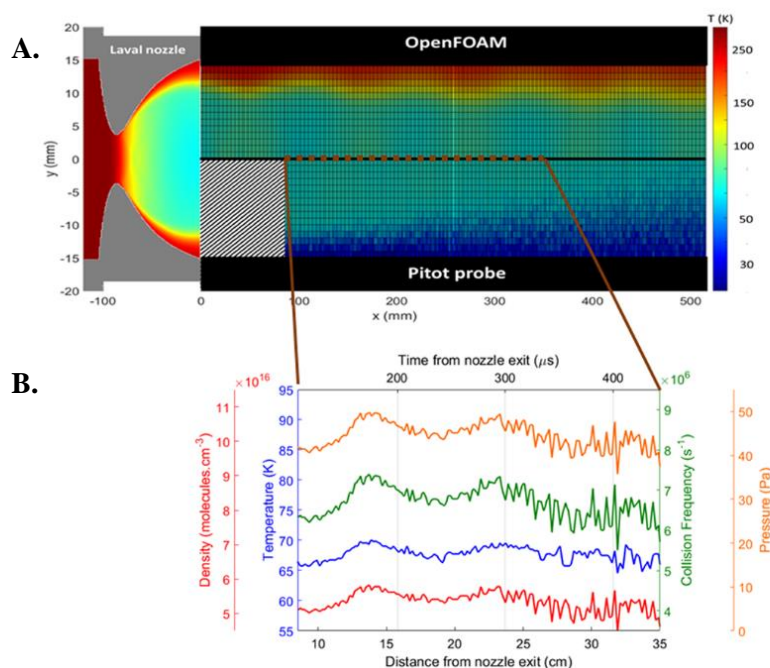
*Figure 2.7 (A) 2D distribution of the kinetic temperature associated with the N$_2$ nozzle from the OpenFOAM simulation (nozzle and top part of the expansion) and the pitot probe (bottom part). The good agreement between the experimental and numerical characterizations is only lowered by the diameter of the isentropic core from pitot measurement which is shrinking with the distance. Indeed, contrary to our simulation, the stagnation conditions are not held indefinitely leading to a shorter flow. (B) Evolution of several indicated thermodynamic parameters along the flow axis measured by a pitot probe. Adopted with permission from Suas-David, N.; Thawoos, S.; Suits, A. G., A uniform flow–cavity ring-down spectrometer (UF-CRDS): A new setup for spectroscopy and kinetics at low temperature. The Journal of Chemical Physics **2019**, 151 (24), 244202.*

CHAPTER 3

UF-CRDS INSTRUMENTATION AND DATA

ACQUISITION

3.1 Introduction

UF-CRDS is a newly built instrumental setup which is complementary to LIF based CRESU machines and the CPUF method[5,6,26] in our group. The latter employs broadband rotational spectroscopy in a pulsed Laval flow. Although microwave spectroscopy is a nearly universal spectroscopic tool, it is limited in its sensitivity. Also, coupling chirped-pulse Fourier-Transform spectroscopy with a high-density uniform flow becomes a challenge when measuring the free induction decay (FID) signals as the higher collisional frequency attenuates the FID. UF-CRDS equipped with a continuous wave near infrared laser enables sensitive and high-resolution detection for complementary species compared to either LIF or CPUF.

3.2 Instrumentation

There are four key parts to the UF-CRDS instrumentation. One is the pulsed Laval flow system (see section 2.3), the chamber, the *cw*-CRDS spectrometer and the photolysis laser. The pulsed Laval system is detailed in chapter 2, therefore in this chapter a detailed description of rest of the instrumentation will be provided. The pulsed Laval flow system is housed in a stainless-steel chamber

of about 1m^3 and a diameter of about 40 cm. This chamber consists of both the cw-CRDS spectrometer and a LIF spectrometer. The main chamber has two parts, one is mobile, and the other is stationary. The mobile chamber is mounted on a railing which can be moved to access the Laval nozzle assembly and the stationary chamber is mounted on to an optical table. The stationary chamber hosts both spectrometers CRDS and LIF and the pitot probe (Figure 3.1).
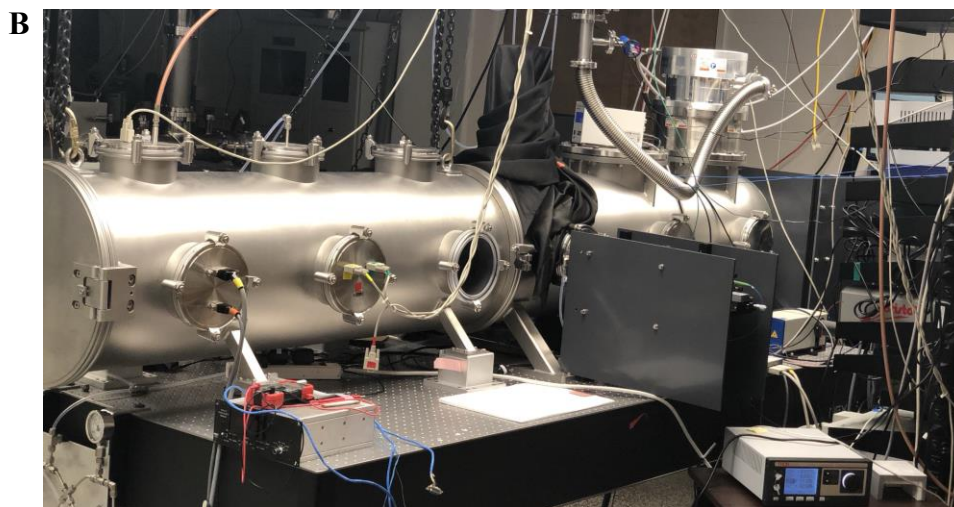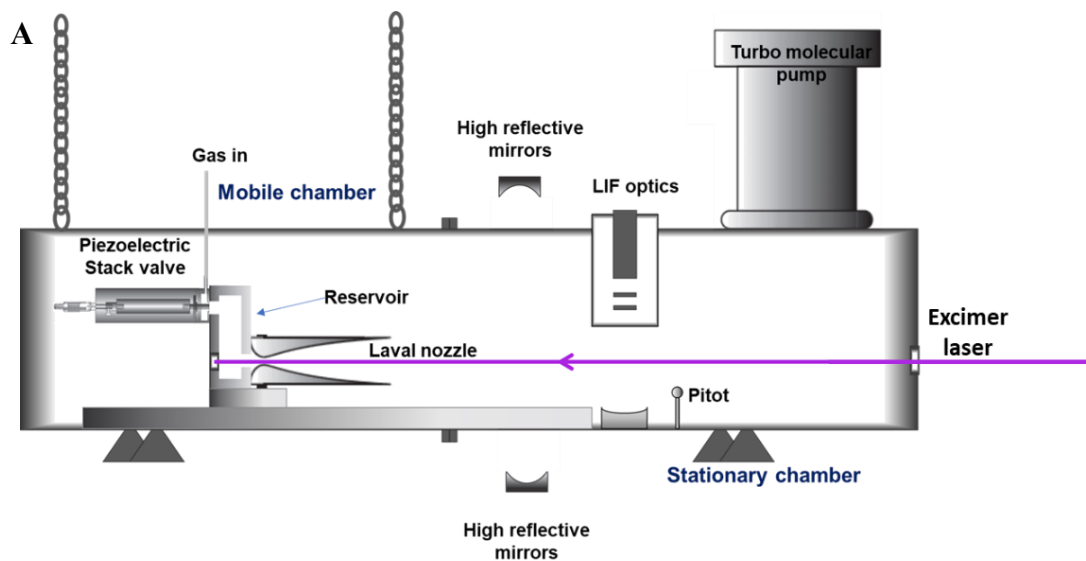
Figure 3.1 A. Schematic illustrating components of UF-CRDS apparatus. B. A picture of the UF-CRDS apparatus

The chamber is pumped using a turbomolecular pump (Osaka TG2400

MBWS, 2400 L/s with N2) backed by a roots dry pump (Osaka ER100D, 1670

L/min with N2).

3.3 *cw*-CRDS spectrometer
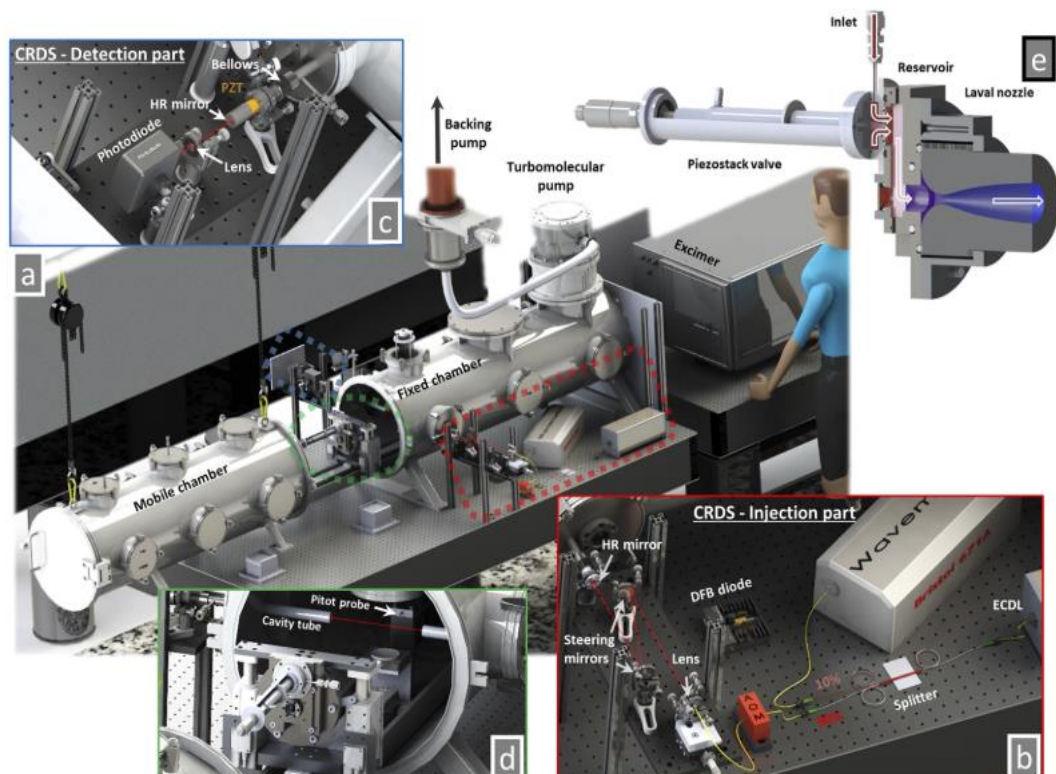
Figure 3.2 Overview of the setup modeled with SolidWorks. The mobile and fixed chambers along with the continuous wave (cw)-CRD spectrometer are lying on a massive optical table associated with passive isolator legs (a). On both sides of the fixed chamber, the injection (b) and detection (c) parts of the CRDS are set. The mobile chamber is hung on a rail and then can be lifted and translated to access the interior of the vacuum chamber and the pulsed uniform flow setup [(d) rearview]. It is composed of three parts (e): the piezoelectric stack valve (PSV), the reservoir, and the Laval nozzle. These are mounted on actuators allowing for an accurate 2D displacement

The cw-CRDS system consists of two planoconcave high reflectivity mirrors (>99.99%) separated by 800 mm. The continuous wave light source is either an external cavity diode laser (ECDL), or a distributed feedback (DFB) diode laser, which could be tuned between 1280-1380 nm and 1411-1419 nm, respectively. Using a fiber optic splitter, 10% of the light is sent to a wavemeter and the remainder is injected into the high finesse optical cavity (F~1900000) via an acousto-optical modulator (AOM). The AOM acts as a fast switch, which operated either by frequency modulation (FM) of the RF applied to it or amplitude modulation (AM). When operated at FM mode the laser is turned off by shifting the laser out of cavity resonance by switching the radio frequency by approximately 5 MHz. At either modes of operation laser is interrupted and the free decay of the light that is injected is allowed. Both high reflective mirrors are mounted on a stainless-steel tube which extends into the chamber until it meets the sheer boundary layers of the Laval flow. The mirrors are isolated from the chamber via a bellows and are flushed using a constant nitrogen flow (maximum of 2 SLM). This nitrogen flow also plays a key role in maintaining

the chamber pressure to achieve the conditions for an ideal Laval flow. The output mirror is mounted on a piezoelectric transducer (PZT).
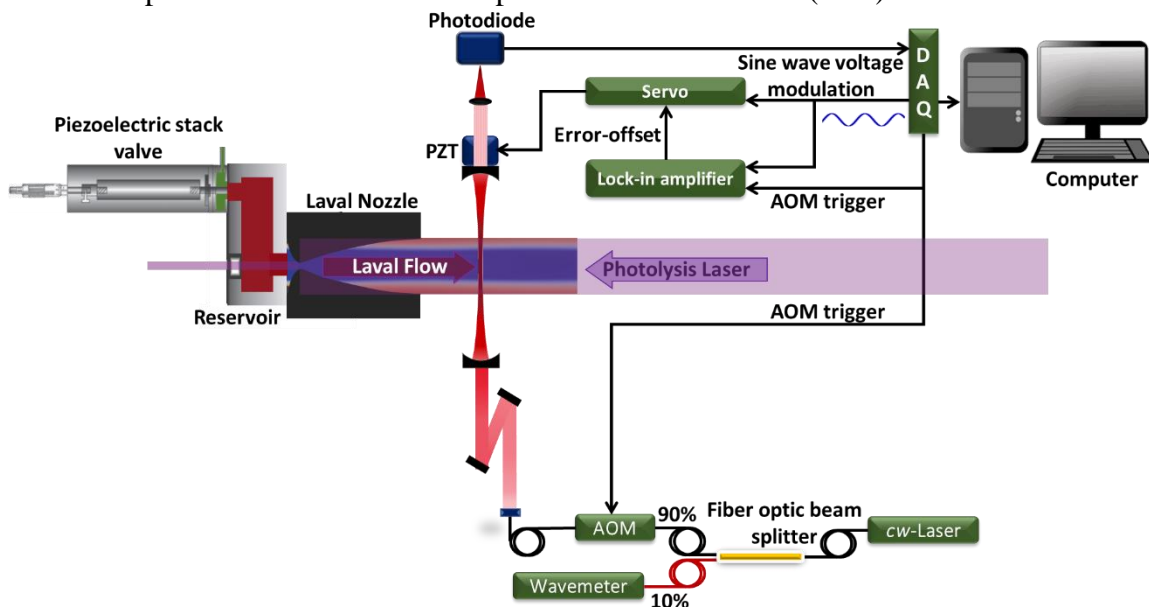
Figure 3.3 Simplified overview of key components of the UF-CRDS apparatus.

3.4 Timing and data acquisition

Synchronization among CRDS events, the gas flow pulse, and the photolysis is crucial in probing the reactants. Initially we adopted the method described by Hippler, M. et al. [27] and implemented successfully by many others[10,28-30], where the cavity is modulated by applying a triangular voltage. The amplitude of the modulation is set such that the cavity length is scanned less than the FSR trapping one TEM_{00} fringe per ramp of the modulation. The modulation frequency operated at 50 Hz and any randomly selected reference fringe will be followed by a second fringe at 20 ms time intervals.

A reference fringe is selected at the desired repetition rate of the PSV by choosing the first fringe following the long delay of the pulse repetition period. A second counter output (ctr1) triggers the PSV typically 16 ms later, allowing
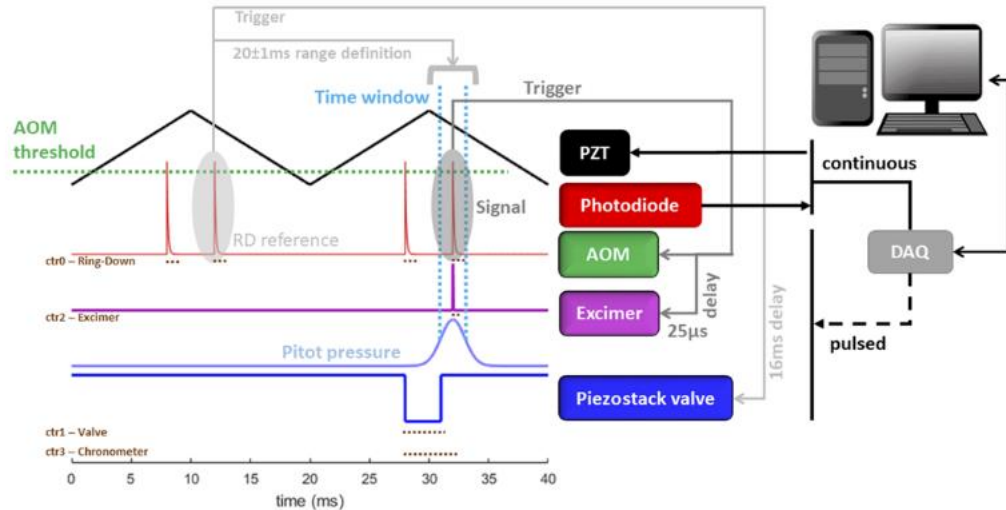
Figure 3.4 Timing and triggering scheme. A fundamental mode is used as a reference to predict the appearance of another one according to the frequency of the PZT. The valve is triggered to produce a steady uniform flow while the decay signal is recorded. Once the expected mode exceeds a threshold set by the user, the AOM switches the beam injection off. The excimer is triggered after a 25 μs delay verifying the background decay conditions. All the trigger and acquisition processes are performed by a DAQ acquisition card driven by a homemade LabVIEW program. The brown dotted lines give the trigger of the different counter outputs provided by the DAQ.

the uniform flow to be established in the viewing region at the anticipated time of the next modulation cycle, typically around 4 ms after the PSV trigger (set according to pitot delay measurement). The first cavity fringe after the valve trigger initiates the excimer laser trigger using a third counter output (ctr2) which can also be delayed triggering the photolysis laser at an adjustable time shortly after the beginning of the ring down acquisition. If the expected cavity mode shows up within a 2 ms window, the recorded ring-down signal is saved and used for the study. The ring-down preceding the one with the synchronized

excimer laser is also saved as an empty cavity reference signal. A fourth and last counter output (ctr3) is used as a clock to monitor the accurate delay between the PSV trigger and the excimer laser trigger.

However, this method of timing and detection is highly susceptible to the vibrations and temperature fluctuations in the lab environment. This limited the throughput of the data acquisition. Therefore, the timing scheme and data acquisition code has been significantly revised to improve stability and throughput with guidance and assistance from Dr. Gregory Hall from Brookhaven. A servo feedback loop was implemented to keep the cavity modulation cycle centered on one transmission fringe, eliminating the slow drift of fringe timing relative to a 50 Hz cavity modulation, even during short scans
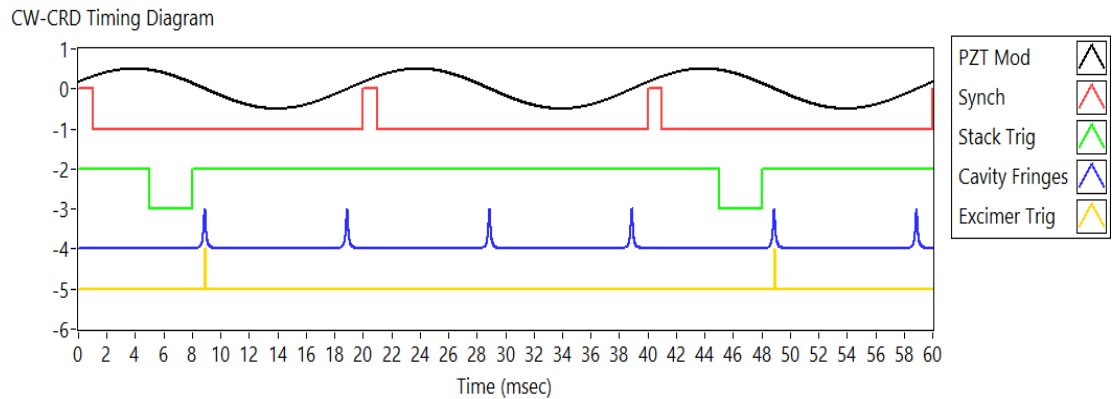
Figure 3.5 Timing signals used in UF-CRDS. Illustration shows Piezo Stack trigger at 25 Hz (divide-by-2) for graphical clarity; actual operation at 5 Hz or 10 Hz (divide by 10 or 5) is generally dictated by limitations of pumping speed. Cavity fringes are shown without typical fluctuations in timing and amplitude.

across Doppler profiles. With this stabilization, the entire pattern of timing signals can be generated in hardware, (National Instruments 6351) without depending on real-time software tests or loops. Figure 3.5 illustrates this timing sequence.

A 50 Hz sinusoidal cavity modulation signal and an adjustable, phase-synchronized timing pulse are generated by continuously retriggered analog outputs from a FIFO buffer in the DAQ multifunction board. The synchronization pulse triggers a counter that provides a pulsed nozzle trigger of adjustable delay and duration at a divide-by-N sub-harmonic of the modulation frequency. The delay is chosen to precede the next anticipated cavity fringe by typically 3-4 msec, the time it takes from the nozzle trigger until uniform flow conditions are established at the downstream position of the CRD beam. The DC bias applied to the cavity piezo transducer is controlled by a servo feedback amplifier (New Focus LB 1005) with an error signal derived from a lock-in amplifier referenced to the 50 Hz modulation signal and processing the detected fringe timing signals (Figure 3.3). When locked, the cavity is modulated with an amplitude somewhat less than one free spectral range, with transmission fringes occurring on average at the plus and minus zero crossings of the modulation cycle, i.e., 100 fringes per second. The photodiode monitoring the transmission fringes and the ring-down signals generate a threshold trigger event to trigger the AOM switching that initiates the ring-down, as well as a clock burst for the 1 MHz acquisition of an analog ringdown signal waveform, and the trigger to start a 25 microsec delay before generating an external trigger for the excimer photolysis laser, having been armed at the time of the last nozzle trigger. The timing jitter between a given pulsed nozzle trigger event and the next cavity transmission fringe is typically distributed around the chosen delay time with a standard deviation of around 1 ms. The trigger threshold for the ring-down signal

is typically set to capture 80-90% of the fringes, so that in addition to the ~1 ms timing indeterminacy for the "right" fringe, the next fringe after the nozzle trigger may be below the triggering threshold. In this case, a subsequent fringe, occurring at a small integer multiple of 10 ms later than the anticipated time will initiate the ring-down acquisition and laser trigger at a time too late to allow interrogation of the gas pulse, which lasts less than 5 ms. To sort the recorded ring-down waveforms according to the time within the gas pulse and to identify those ring-down signals that are not synchronized with the gas pulse, a timer in the DAQ multifunction board is started with the nozzle trigger and stopped with the photolysis laser trigger, derived from the photodiode threshold detection. All of these timing tasks are defined as asynchronous processes, running autonomously on the DAQ multifunction board.

The data acquisition is interrupt-driven (referred to as dynamic events in LabView), reading a new timer value when the data is ready (at the repetition rate of the nozzle and photolysis laser) and reading a new ring-down waveform whenever a complete ring-down data buffer is ready to read, (at approximately 100 Hz). We use a data queue to combine each ring-down waveform and its system timestamp with a copy of the most recently recorded timer value and its timestamp and add this cluster of data as the next element in the data queue. In this way, the ring-down data associated with the gas pulse and photolysis laser is evident as the first one with a new value of the timer reading, which in turn can be used to accumulate ring-down data in bins according to their time relative to the start of the gas pulse. The ring-down events not associated with a gas pulse

can be combined to give an averaged background ring-down signal for reference (Figure 3.6). All the time-critical data acquisition steps are performed in an event-driven producer loop that adds records to the data queue, while all diagnostic, plotting, binning, and storage tasks can be done in an asynchronous queue-consuming loop, tolerant to processing lags or occasional CPU-heavy tasks without losing or mislabeling data. At a fixed probe wavelength, signal acquisition proceeds by retrieving the oldest element of the data queue and deciding if it is the first record with a new timer value. If so, the timer value is used to choose which 0.2 ms-wide time bin to accumulate the ring-down signal in, incrementing the number of hits in the appropriate time bin and updating the sum of ring down signals in that bin. All other ring-down signals are instead accumulated in a running average of background ring-down curves (Figure 3.6). Once a desired number of averages has been accumulated, a file is saved with the time-sorted ring-down events associated with a gas pulse and photolysis laser, the background average ring-down signal, and the rest of the relevant experimental parameters under computer control. A scanning mode has also been implemented, which repeats this process at each step of the probe laser and saves a catenated file of similar contents at each dwell frequency of the scan.

3.5 Applications of the UF-CRDS apparatus

The performance of the UF-CRDS apparatus was tested in both spectroscopic and reaction kinetics measurements. In this chapter we explore the capabilities of the UF-CRDS apparatus.

3.5.1 Spectroscopy of neutral molecules

CRDS is a powerful tool to study the spectroscopy of neutral molecules and radicals at low temperature. Many studies have successfully combined a CRDS with free jet expansions, however, strong temperature and density gradients encountered within these expansions make an accurate characterization of the probed environment problematic. Also, the Doppler broadened line shapes get complicated due to boundary layer contributions and the transverse flow velocity variation over the course of a free jet expansion[31]. The pulsed Laval flow provides an environment where the density and the temperature are uniform which will enable accurate spectroscopic characterization without any artifacts. The ability to scan the wavelength across a rotational line and use CRDS to measure the absorption makes CRDS a great approach to investigate Doppler
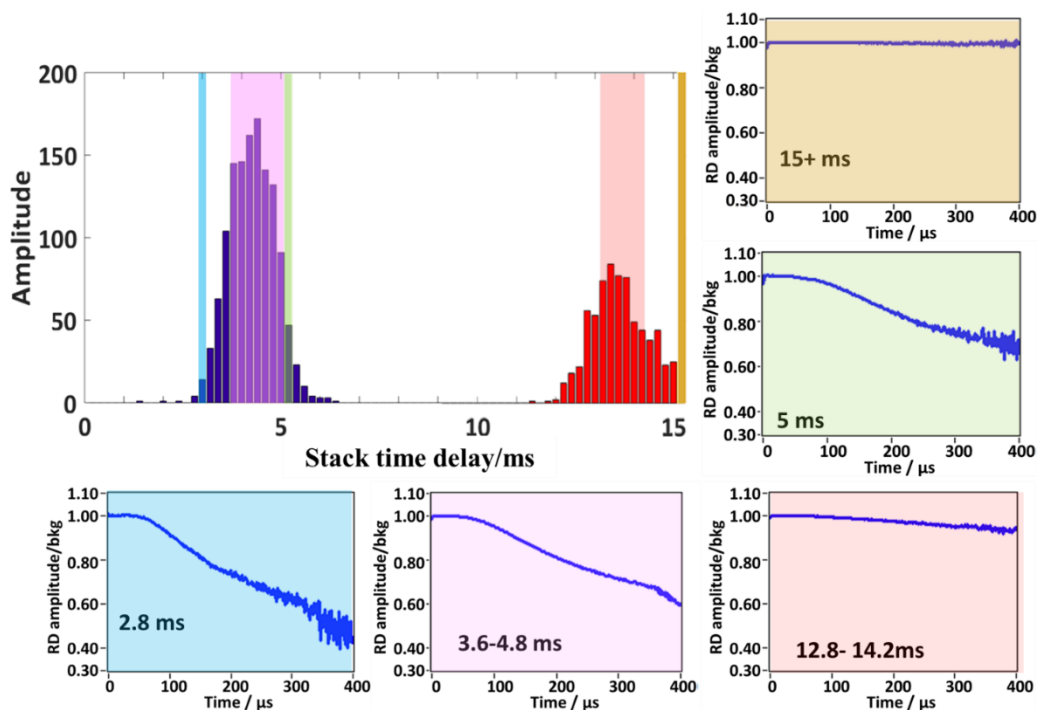
Figure 3.6 Data sampling at fixed wavelength at different time bins with respect to the stack time delay.

broadened line shapes of rotational lines of absorbing molecules in a uniform flow[32-35]. Figure 3.7 presents the recorded spectrum of acetylene (C_2H_2) on the $1_0^2 5_0^1$ overtone combination band.

This spectrum has been recorded far from the optimal condition and shows a minimum absorption coefficient of 4×10^{-8} cm^{-1}. We usually can reach 2×10^{-9} cm^{-1} after averaging only 3 ring-downs. Because the actual region of interest, that is to say, the isentropic core, is only a confined part of the total cavity length, the effective minimum absorption coefficient currently reachable by the UF-CRDS is around 8×10^{-8} cm^{-1} or a fractional absorption of 0.2 ppm per pass. In Figure 3.7, we can notice that the intensity ratios are not perfectly reproduced and worse for high J values. Despite the nitrogen flush sent in the cavity tubes, contributions from the boundary layers can still be recorded.
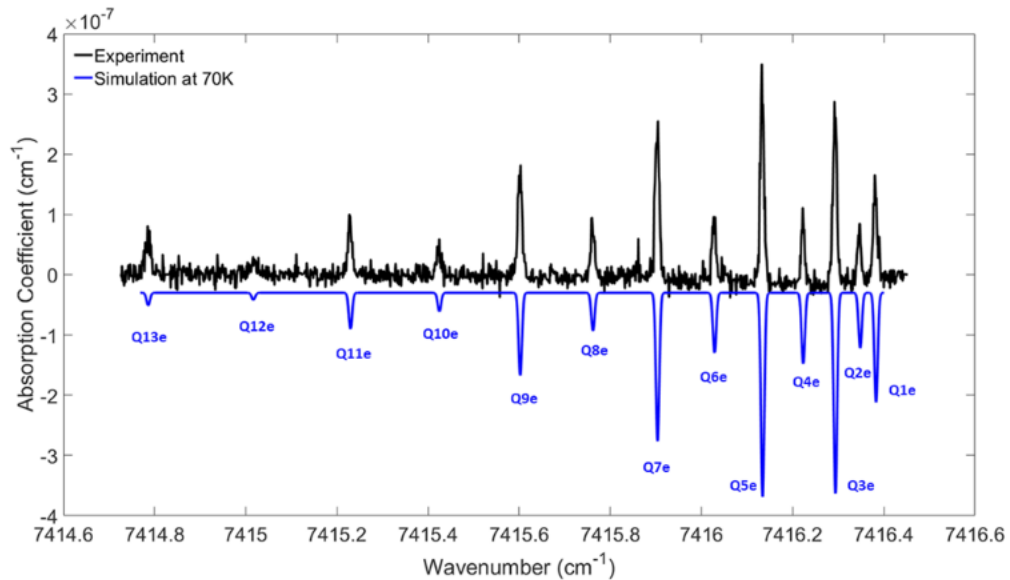
Figure 3.7 $1_0^2 5_0^1$ overtone combination band of acetylene in 70 K flow. Black: recorded spectra using UF-CRDS methos. Blue: Simulated spectra using the HITRAN database

3.5.1.1 Boltzmann plot

To retrieve the rotational temperature, a two-slope analysis was performed with a Boltzmann plot (Figure 3.8) We use the high J values to determine the contribution of the warmer gas on the low J value lines which mainly come from the isentropic core. Once subtracted, we found a rotational temperature of 66.2 ± 5.7 K in the range of the kinetic temperature given by the pitot probe (68± 2 K) within the isentropic core. Extracting the kinetic temperature from the linewidth is not straightforward due to this hot contribution within all the transitions, even for the first J value for which it counts for 30% of the line area. This contribution could be further limited by extending the cavity tubes closer to the isentropic core and/or increasing the flow flushing the cavity. However,
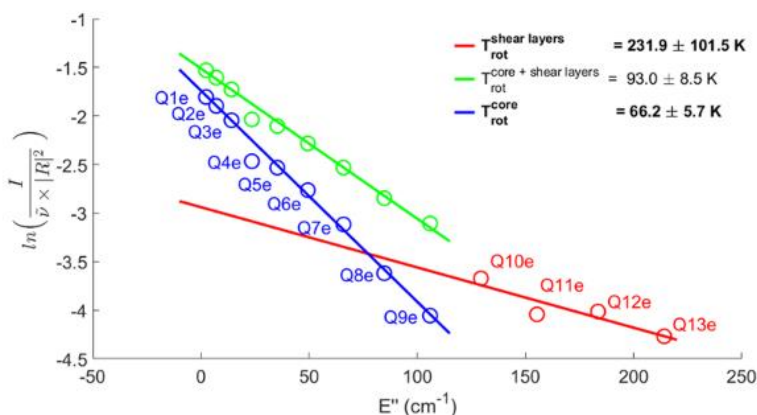
Figure 3.8 Boltzmann plot from the acetylene spectra (Figure 3.7) with I, v, R, and E'' the area, the wavenumber, the total moment, and the lowest energy level of the transitions, respectively. The red points and slope are related to the boundary layer contribution, while the green data come mainly from the isentropic core. The blue trace corresponds to the intensity of the lower J values (green) after subtraction of the hot contribution by extrapolating the intensity contribution from the high J values (red). The values are in the 95% and 68% tolerance intervals for the isentropic core and the boundary layers, respectively.

such limitations do not occur when using a photolysis probe to trigger the study because the target is only produced within the isentropic core.

3.5.1.2 Doppler broadened line shapes

Given the high spectral resolution of the cw laser, careful measurement of a line shape can also be used to measure the local rotational temperature. We applied this to C_2H_2 focusing on measurement of a lower rotation level of the $1_0^2 5_0^1$ overtone combination band. We obtained the Gaussian line shape for the Q3 rotational level (Figure 3.9). We examined two different flow conditions, 15 K and 25 K with He gas then used background subtracted absorption spectra to calculate the rotational temperature using a simple Gaussian fit. (Equation 1)

$$\Delta f_{FWHM} = \sqrt{\frac{8kT\ln 2}{mc^2}}\, f_0 \qquad (1)$$

Where *m* is the mass of the molecule, *T* is the temperature, *c* is speed light, *k* is the Boltzmann constant, f_0 center frequency and Δf_{FWHM} is the standard deviation of the frequency at full width at half maximum of the Gaussian fit for the line shape.
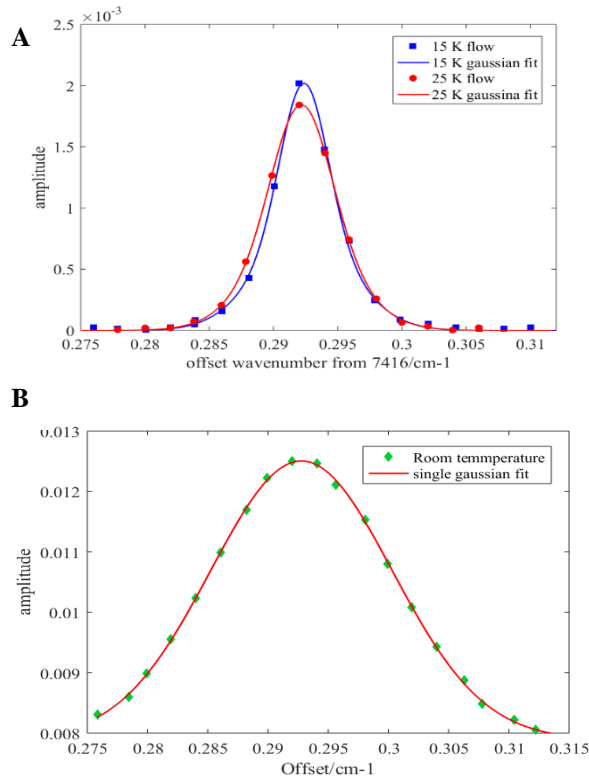
Figure 3.9 Doppler line shape for Q3 line of $1_0^2 5_0^1$ overtone combination band and the Gaussian line shape fit using summation of two concentric Gaussian fits. A. spectral lines measured in of 15 K and 25 K pulsed Laval flow. The solid (blue) square is the raw data points in the 15 K flow and the solid circles (red) for the 25 K flow, the solid lines connecting the data points is the summation of two concentric Gaussian fits. B. is the spectral line recorded using a slow flow cell at room temperature and the single Gaussian fit corresponding to a 295 K temperature profile.

The measured line shape was fitted using two concentric Gaussian shapes and the shape recorded in the 15 K flow has a major contribution from 16 K and a minor at 73 K (0.4%) whereas these values for the 25 K flow was 26 K and 215 K (0.2%) respectively. We also measured the line profile at room temperature and were able to retrieve 295 K using a single Gaussian fit.

39

3.5.2 Spectroscopy of CN(v=1)

The chief radical species of interest here is vibrationally excited CN formed by photolysis of cyanogen bromide (BrCN) using an excimer laser operated at 248 nm (70 mJ/pulse). This molecule has relatively strong transitions in the frequency range of our DFB laser. In Fig. 3.10 we show the simulated absorption spectrum on the (2-1) vibrational band of the $A^2\Pi$-$X^2\Sigma^+$ electronic transition. generated using PGOPHER with the spectroscopic constants reported in literature[36]. The DFB diode laser was able to tune between multiple rotational lines. However, scanning the spectrum across all the spectral lines is very time consuming.
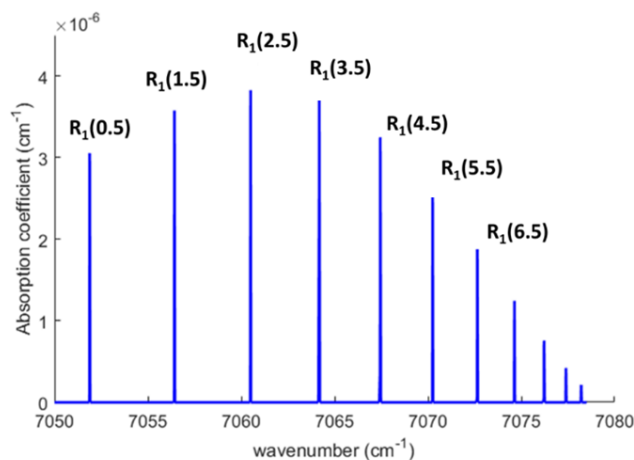
Figure 3.10 PGOPHER simulation (blue) of the R1 branch of CN (v = 1) electronic transition $A^2\Pi$–$X^2\Sigma^+$.
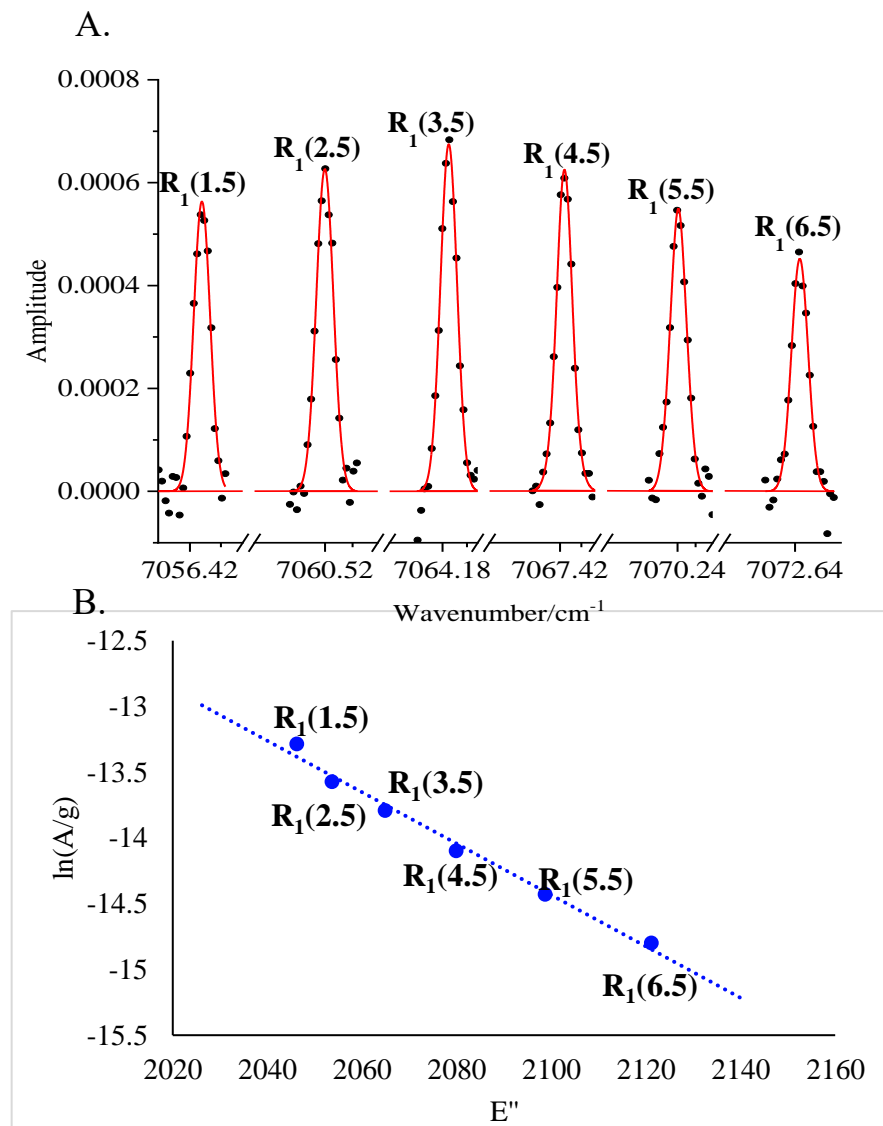
Figure 3.11 A. Recorded spectral lines for j=1.5 through 6.5. The black points are the raw data points, and the red solid line is the Gaussian fit. B. Boltzmann plot from the CN(v=1) spectra recorded with A, g and E″ the area, the degeneracy, and the lower state energy of the transitions, respectively. The measured temperature from the slope is 73.8±8.4 K.

The spectroscopic scans done for each rotational line from j=1.5 through to 6.5 in the 70 K nitrogen Laval flow and Boltzmann plot constructed are shown in figure 3.11. The temperature calculated from the slope of the plot gives us a value of 73.8±8.4 K, which is in close agreement with the flow temperature recovered from pitot measurements. However, the temperature calculated from

41

the Doppler line (the red solid lines from figure 3.11 A) width corresponds to a warmer 120-140 K range of temperatures compared to the flow temperature.

3.5.3 Reaction kinetics of CN(v=1) and propene

As one of the first reaction kinetics measurements we choose the reaction between vibrationally excited CN(v=1) and propene as test case study. We use the SKaR method to measure the rates of the reactions for the first time in a Laval flow. Here, we measured the reaction rate between CN (v = 1) and propene seeded in a uniform flow of N_2 at 68 K. We follow the rate of loss of the radical by probing the center of the rovibrational line $R_{1e}(5.5)$ of the $A^2\Pi$-$X^2\sum^+$ electronic transition at 7070.2422 cm^{-1}. Although not the most intense line at 68 K, it has the advantage to be close to the center wavelength of our DFB diode, thus maximizing the laser intensity to inject into the cavity.

CN radicals are produced in the vibrationally excited state by photolyzing cyanogen bromide (BrCN - Sigma Aldrich, 97%) at 248 nm and 25 mJ per pulse. Although the absorption cross section of BrCN is one order of magnitude weaker at this wavelength compared to 193 nm[37,38], it has previously been demonstrated that excited vibrational states are more efficiently populated for a photolysis probe operated above 240 nm[37] and drops with decreasing photolysis wavelength[39,40]. Moreover, the initial rotational distribution, although very hot, is much less so at 248 than 193nm We assume the vibration will not relax during our recording time due to a negligible quenching of CN(v=1) by N_2[41]. Moreover, quantum calculations based on a VCC-IOS approach demonstrated the

predominance of elastic rate coefficients over a wide range of kinetic energy (15000 cm^{-1})[42].

N$_2$ gas is passed over a sample of finely ground BrCN powder packed in a home built stainless steel metal bubbler. The bubbler is placed in a temperature-controlled water bath and the temperature is set at 23°C to maintain a constant concentration of the precursor molecules (1%). A 25% propene mixture in N$_2$ was prepared for mixing with additional N$_2$ to achieve the target concentrations for the pseudo-first-order measurements. The compositions of the injection gas mixture for the kinetics experiments were adjusted using mass flow controllers (Alicat, MCS type). The uniform expansion, characterized by CFD and Pitot probe (see figure 2.7), is defined by a 2 cm diameter isentropic core at 68±2 K and 5.4±0.3 × 10^{16} molecule. cm^{-3} total density.

The CN concentration is calculated from the absorption coefficient of the CRDS signal and the estimation of the absorption cross section. Here, the rotation is equilibrated to the translational temperature (T$_{rot}$=T$_{kin}$=70 K) while the excited
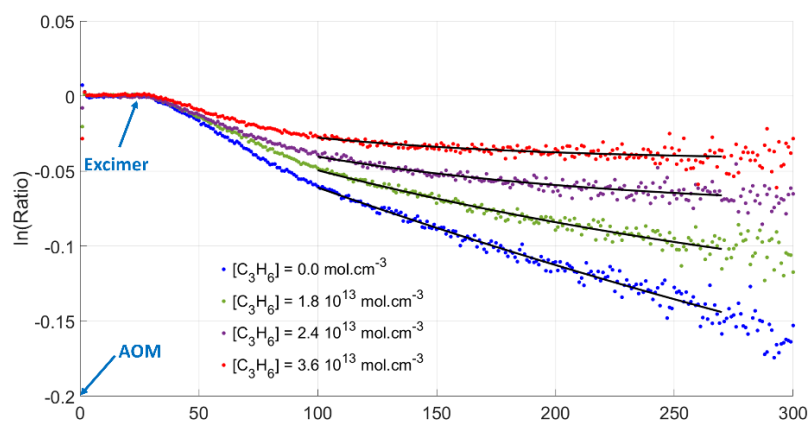
Figure 3.12 – Ratio of the CN signal over the empty cavity for four different concentrations of propene. The logarithm of this ratio is then fitted by a simple exponential to retrieve the pseudo first order constant of the reaction for each propene concentration.

vibrational states do not relax within our recording time (see above). We estimated a vibrational temperature of 2000 K in order to retrieve the v=1/v=0 ratio (0.24) observed by Russell et.al.[37]. This way, through the rotational and vibrational partition functions (we assume that CN is mainly in its electronic ground state), we computed an out of equilibrium absorption cross section shaped with the appropriate Gaussian function related to the kinetic temperature. We finally found a density of CN (v=1) of 2.2×10^{10} molecules.cm^{-3}. Thus, because the population of the higher vibrational states are negligible[39], the total concentration of CN is estimated to be around 1.0×10^{11} molecules.cm^{-3} which is slightly lower than an estimation based on the excimer fluence (2.5×10^{11} molecules.cm^{-3}).

The flow is probed perpendicularly by the cw-CRDS at 15 cm from the output of the Laval nozzle leading to a hydrodynamic time greater than 190 µs (Figure 2.7). The reaction is investigated in the pseudo-first order approximation where the CN concentration (see above) is negligible compared to propene ($> 10^{13}$ molecules.cm^{-3}). The pseudo-first order constant k_{1st} is calculated using the SKaR approach detailed above. For each C_3H_6 concentration an average of 200 measurements of signal and background are recorded to plot the logarithm of the ratio to be fitted (Figure 3.12). The excimer is fired 25 µs after the AOM triggers the CRDS measurement which leads to an expected ratio equal to 1 (signal and empty cavity overlap) over the initial time range.

The exponential decay (ln(Ratio)) is fitted from 100 to 270 µs. The upper limit corresponds to the hydrodynamic time of the flow extended with the region

inside the nozzle which can be considered as uniform. The lower limit is shifted by 75 µs from the excimer pulse due to the non-exponential behavior of the curve in this time window. Because the CRDS is not affected by the UV light as it could be in a LIF measurement where some scattered light could play a role in the first µs of the fluorescence, the most likely explanation for nonexponential behaviors is the rotational relaxation. This is a field of interest by itself[43]. Although the 248 nm photolysis will lead to a nascent rotational temperature lower than its counterpart at 193 nm, the rotational distribution is peaked around N"=45[37] corresponding to 4000 cm^{-1}. The exponential behavior of the relaxation of the higher rotational states to the probed ones would alter the initial profile, of course. But classical collision theory under these conditions predicts a CN radical should undergo 7 million collisions per second, which means that before the recording, each of them will experience around 500 collisions. Hay et al. have measured rotational relaxation rates in a variety of gases including N_2, and found bimodal distributions at early times, with, for N_2, 2/3 of the rotational excitation removed in 150 collisions[44]. So, by comparison with our system, CN should be rotationally thermalized even at the start of the data recording. This is only a rough estimation that does not consider the bimodal distribution, where the highest rotational levels relaxed far slower than the lower ones, nor does it consider possible faster relaxation with increasing propene concentration. This relaxation is further confirmed by the measurement of J=1.5 through 6.5 of CN(v=1) and the Boltzamann temperature (figure 3.11) reported similar to the kinetic temperature from the Pitot probe (figure 2.7) and the rotational

temperature of acetylene (figure 3.8). These intensities are recorded in the same conditions as the kinetics experiment where the signal is fitted between 75 and 245 µs after the photolysis pulse.

The relaxation process remains the preferred explanation for the early non-exponential ratios. Current investigations suggest the majority of is caused by diffusion into the probing region due to mis-alignment of the excimer laser with respect to the CRDS probe. A small adjustment to the excimer alignment and the loose focusing could help to eliminate this effect to the most part in 70 K flow. However, this effect remains prominent in lower temperature flow which will be discussed in chapters ahead.

The pseudo first order constant has been measured for different densities of propene from 6.0×10^{12} to 5.0×10^{13} molecules.cm^{-3} (figure 3.13). At higher
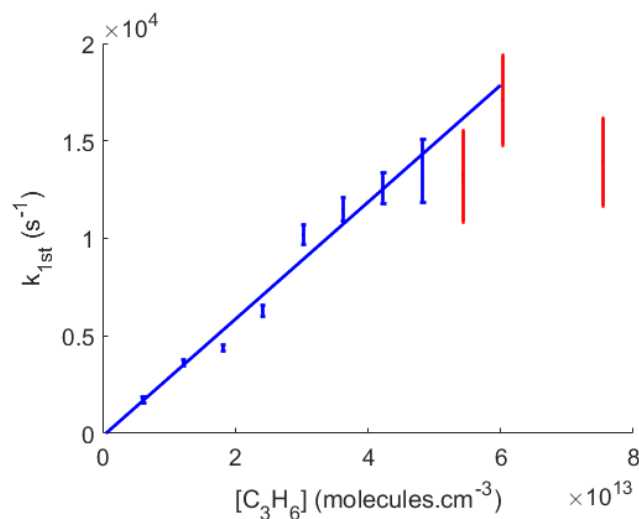
Figure 3.13 - Second order plot for the reaction of CN (v=1) with propene. The blue points are taking into account to calculate the reaction rate while the red one are rejected mainly due to the complete reaction of CN within or time range. The statistical error is estimated at 4.0 x 10^{-11} cm^3.molecules^{-1}.s^{-1}, 2σ level. These measurements have been obtained from the fit of the logarithm of the ratio between the reaction signal and the empty cavity (see fig. 3.12).

density, in addition to the formation of propene clusters as mentioned in previous studies[2,45], almost all CN has reacted in the time range we probe.

To date, there is no clear evidence of the pressure dependence of the reaction between CN and propene in Laval flows. The reaction proceeds by CN addition to the double bond at the C1 or C2 carbon forming a strongly bound (> 2 eV) intermediate. This may eliminate H or CH_3 or be stabilized by a third-body collision. Some questions have arisen concerning the pressure-dependent branching between H and CH_3 elimination[46-49] but we do not monitor products so we will not be sensitive to this. Furthermore, our pressure and temperature conditions are similar to Morales et al.[50] who found no difference in the CN decay rate by varying the pressure by a factor 10 at 298 K and 2 at 52 K. This is consistent with the master equation modeling reported by Gannon et.al. that suggested only 2% adduct formation at 1 Torr and 90 K, and none at 0.5 Torr[49]. To be noted, no pressure dependence has ever been observed for different small hydrocarbons in CRESU experiment conditions[51].

From the analysis, we found a reaction rate of $(3.0 \pm 1.2) \times 10^{-10}$ cm^3.molecule^{-1}.s^{-1} (figure 3.14). This rate is higher than the classical hard sphere collisional limit ($\approx 10^{-10}$ cm^3.molecule^{-1}.s^{-1}) as observed in other studies[52] highlighting the importance of the long range attraction better described by the capture rate theory[53]. We obtain an intercept of -150 s^{-1} showing the CN (v=1) time dependence is fully dominated by reaction with propene and diffusion is negligible. The uncertainty evaluated for this experiment includes statistical and systematic errors. The statistical uncertainties contain the unweighted least-square analysis (2-sigma) of the second order plot multiplied by the appropriate Student's t-factor (2 sides) corresponding to the sample size. The systematic error takes into account the mass flow variation of the different reactants, the variation of density and temperature that might be experienced by the uniform flow and the other possible reactions notably with impurities (reaction rates
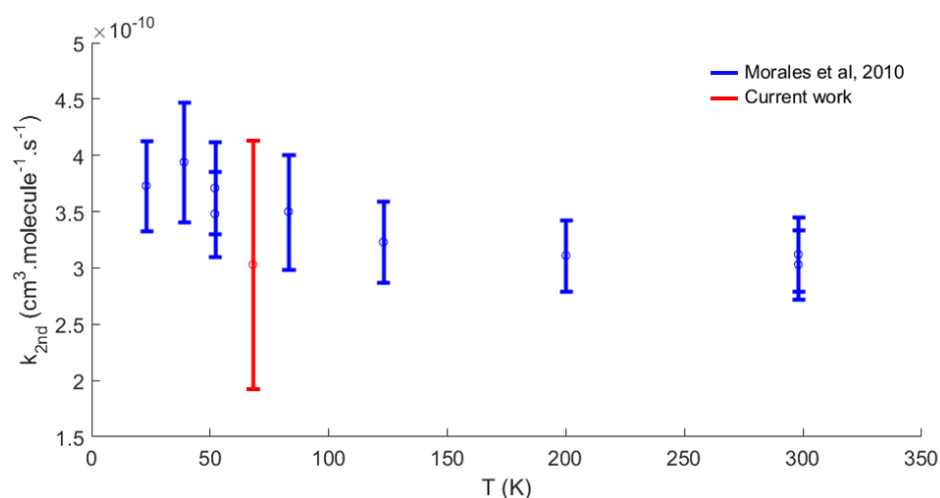
Figure 3.14 - Comparison of the reaction rate of CN + propene between our current study at 70 K where CN (v=1) is probed by cw-CRDS and Morales et al, 2010 for CN (v=0) probed by LIF.

between CN and BrCN is negligible[47,48]). This uncertainty has been safely estimated at 10% maximum as in many of the similar studies.

In spite of an uncertainty twice the value obtained from LIF experiment due to a smaller propene density range and a lower number of k_{1st} values, our reaction rate seems in a good agreement with a previous experiment probing CN (v=0) by LIF in a uniform flow as well[50]. This latter study has been performed over a wide range of temperature between 22 and 300 K. The slight negative temperature dependence associated or not with an upper limit is typical of a reaction between CN and small unsaturated hydrocarbons such as acetylene[51], ethylene[42,51], allene[54,55], methyl acetylene[50,55],1-Butyne[50] while there are some exceptions like 1,3 butadiene[54,56] which follows an Arrhenius behavior.

The absence of reaction rate discrepancy between our data and the previous LIF study (fig. 11) suggests that this low temperature reaction rate is independent of the vibrational state at least for v=1. The dependence of the reaction rate on CN vibrational state has been debated for different reactants with no clear conclusion. The reaction with O_2 for example which has been one of the first reactants associated with CN, has been first determined as faster in presence of vibrationally excited $CN^{[3,41,57]}$ while other studies[58-60] found an opposite behavior resulting from a higher rate of complex formation for CN (v=0). The second most studied species for its astrophysical interest is H_2. A consensus emerged suggesting that vibrationally excited CN leads to a faster reaction in that case[41,60-63]. The same conclusion arises from two studies associated with

methane[41,64]. However, Herbert et al. performed a broader kinetics study with saturated and unsaturated hydrocarbons (including propene)[65]. Only saturated hydrocarbons (methane and ethane) were studied in conjunction with CN (v=1) with reaction rates comparable to CN (v=0) as predicted by the vibrationally adiabatic transition state theory[66] and in relatively good agreement with a previous study[67]. All of these measurements have been performed at room temperature or higher (up to 1000 K). To our knowledge, the influence of the vibrational state of CN has not been studied at low temperature. Below room temperature, we could only find data for the reaction $CH + D_2$[68] with a reaction rate 20% faster for CH (v=1) over the entire temperature range from 88 to 584 K, suggesting that for that system the room temperature data could be extrapolated to low temperature. Further investigation would be needed to conclude about the influence of the vibrational state on the reaction rate at low temperature. We note that the reaction rate determined here includes vibrational quenching, which could play a role as initially formed adducts could decay back to reactants but with exchange of vibrational energy from CN to propene.

CHAPTER 4

LOW TEMPERATURE REACTION KINETICS

OF CN(v=1)

4.1 Introduction

Reactions of CN have considerable importance in understanding formation of nitrogen rich compounds in many different environments including combustion, interstellar clouds, and the atmospheres of planets and their moons. Therefore, there is a great interest in studying reactivity of CN with wide varieties of counter reactants in varying reaction conditions. The recent development in the CRESU technique using LIF has enabled studies of reaction of CN with various co-reactants including small molecules such as O_2, H_2, small hydrocarbons, NOx, amines, and many more. The CRESU technique has been combined with robust LIF detection of CN, where typically the (0,0) band of the $B^2\Sigma$-$X^2\Sigma$ transition is excited at ~387 nm with fluorescence is detected on the (0,1) emission at 420 nm. This created a path to investigate extensively these reactions at very low temperatures down to 15 K. However, the literature in low temperature kinetics have been primarily dominated by CN(v=0) even though the there is sufficient evidence of existence of vibrationally excited species in many reaction environments[39,40,59,64,69-71] and interesting issues are raised in comparing the rates of the vibrationally excited CN with CN(v=0). It is important to understand the role of the vibrationally excited reactants as the overall reaction rate either can be controlled by reactive processes, non-reactive

relaxation, or significant contributions from both[3,62]. Our ability to detect CN(v=1) coupled with the CRESU system permits us to explore the reactive and non-reactive relaxation rates of vibrationally excited CN with O_2 and NO respectively at temperatures 70 K and 24 K.

4.2 Experimental methods

Our principal source of CN in these experiments is cyanogen bromide (BrCN). Photolysis of cyanogen bromide has been studied extensively[37,72] and we use an excimer laser operated at 248 nm to produce CN from BrCN as described in Chapter 3. The literature suggests that the vibrational excitation is higher is 248 nm photodissociation of BrCN compared to that at 193 nm[37,40]. The 248 nm excimer was operated at average power of 80 mJ per pulse. The excimer is aligned along the axis of nozzle and counterpropagates to the flow. To maximize the overlap of the CRDS probing region and the photolysis volume, the rectangular shape of the excimer is rotated and loosely focused vertically using a cylindrical lens. In order to minimize the power loss of the excimer due to attenuation due to absorption by BrCN in the downstream of the Laval flow, the excimer window is mounted at the end of a cylindrical tube that extends into the vacuum chamber. This tube is around 60 cm long and reduces travel path of excimer laser through the flow.

The BrCN is ground into a fine powder and placed in a metal gas bubbler. The bubbler is placed in a temperature-controlled water bath of about 21-22 °C. The carrier gas is passed through the bubbler at a constant pressure. The output from

the bubbler is sent through a flow controller and mixed with the co-reactant prior to filling up the reservoir to the Laval nozzle. In the premixing we use three flow controllers (Alicat MCS type, 1SLPM,2SLPM and 10sccm). One controls the BrCN-seeded gas from the bubbler, a second with pure carrier gas acting as a diluent and third controlling the co-reactant input. As BrCN has a high vapor pressure at room temperature and limited ability to supply a higher backing pressure the diluent gas flow plays critical role in maintaining low BrCN partial pressure in the flow. The ultra-pure research grade carrier gases Ne (NOVA gas), and N_2, O_2 (AirGas) and NO (Praxair) were used as purchased without any further treatment. Moreover, a premix of the co-reactant in the carrier gas with a partial pressure of about 25-30% is used.

The loss of CN(v=1) is measured by probing either rotational line j=5.5 at 7070.240 cm^{-1} or j=2.5 at 7060.520cm^{-1} for 70 K and 24 K flow conditions respectively. 7070 cm^{-1} is the preferred wavelength to operate as the DFB diode laser operates at its optimal conditions and has the most efficient light coupling to the cavity, which in turn results in intense and stable cavity fringes. This enables efficient data acquisition. However, although tuning the DFB laser to 7060 cm^{-1} raises challenges, the sampling throughput could be maintained around 60% which is reasonable to maintain the cavity lock position as well as to complete the reaction for a range of concentrations of co-reactants. The data is acquired according to the revised method explained in Chapter 3. The ratio of the foreground and background ringdowns is averaged for two time bins (400 us). The time bins are selected within the uniform range of the flow pulse which

centers around 3.6 ms from the piezoelectric stack valve trigger pulse. The pitot measurements and the ringdown measurements made between 3.2-4.2 ms show the flow to be at uniform conditions there.

4.2.1 SKaR analysis

Background normalized ringdown is used to retrieve the pseudo first order decay as explained previously with the following modifications. Instead
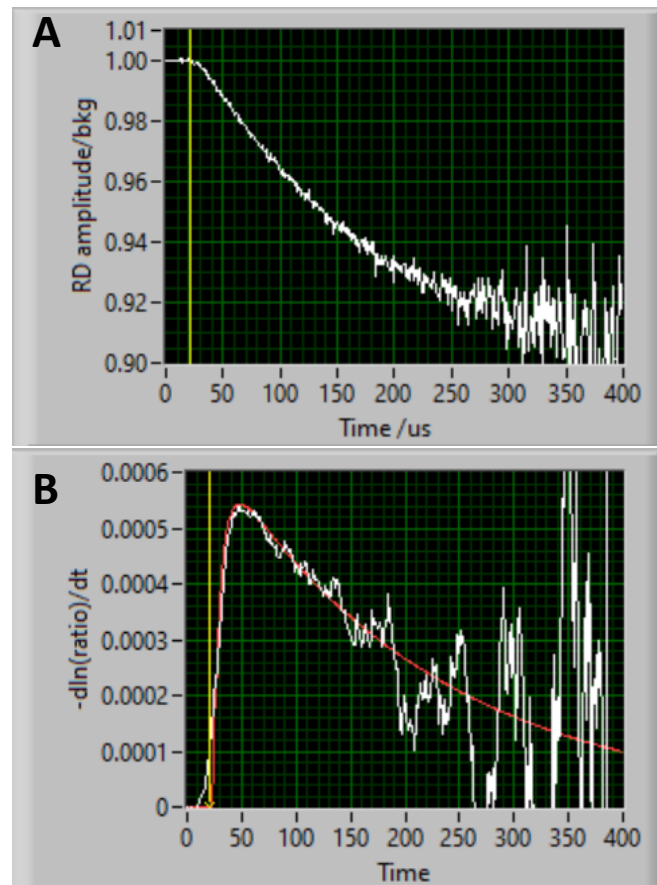
Figure 4.1 A. Background normalized ringdown decay. B. Negative derivative of the natural logarithm of the smoothed data from A (white) and the rise-fall fit (red) where time limits are set at 23 and 180 μs for the lower and the upper limits.

of, fitting the background normalized data from 100-270 μs as explained in chapter 3, we use a parameterized fitting function transformed according to the equation 13 from chapter 1.

$$[A](t) = \frac{1}{c\sigma} \frac{L}{L_A} \frac{-d \ln[Ratio(t)]}{dt} \tag{1}$$

Where, *[A](t)* is the absorber concentration at time *t*, *L* is the cavity length, L_A is the length over which the absorber is present, *c* is the speed of light and σ is the absorption coefficient. The white trace in figure 4.1 A represents the background normalized ratio of the ringdown time. The negative derivative of the natural logarithm of the smoothed data from figure 4.1 A is plotted in figure 4.1 B (white). To extract the time dependent absorber (CN(v=1)) kinetics we have chosen a function which is a difference in exponentials that give rise to a rise and a fall rate. (Equation 2)

$$rise\ fall = a \left(\left(e^{-rise \times t} \right) - \left(e^{-decay \times t} \right) \right) \tag{2}$$

The fitted curve in figure 4.1 B (red) represents the optimized rise fall obtained. The rise fall amplitude parameters were adjusted to perform the least square fitting to obtain the function for the time dependent change in concentration of vibrationally excited CN(v=1). The rise rate approximates the growth of CN(v=1) due to rotational thermalization and the decay rate is the loss of thermalized CN(v=1) due to reaction. The lower limit of the time interval chosen for the fit is set at 23 μs at which the excimer is fired, and the upper limit is chosen based on the hydrodynamic time of the uniform flow.

4.3 Reaction of CN(v=1) with O_2

There are many studies of the reaction of ground state CN and O_2 at temperatures ranging as high as 4000 K to as low as 13 K, and theoretical studies to support these measurements[2,14,53,73-76]. It is considered to be one of the classic radical-radical reactions and one of the very first reactions studied using the CRESU apparatus in Rennes[14].

The reaction between CN and O_2 can lead to three different exothermic product

$$CN + O_2 \longrightarrow NCO + O \qquad \Delta H = \text{-56 kJ/mol} \qquad (1)$$
$$CO + NO \qquad \Delta H = \text{-456 kJ/mol} \qquad (2)$$
$$N + CO_2 \qquad \Delta H = \text{-354 kJ/mol} \qquad (3)$$
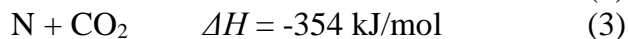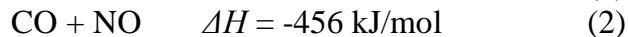
channels.

Among the three pathways, the dominant reaction channel is that forming products NCO and O (1) while the channel leading to N and CO_2 (3) is not observed. The reaction pathway of CN + O_2 can take place on potential energy surfaces of doublet or quartet spin multiplicity with the latter considered non-reactive. On the doublet surface, the reactants can approach without a barrier to form a bent NCOO complex bound by 45 kcal/mol, then to products via a series of barriers and minima. This leads to the least exothermic pathway among three channels to be the most dominant pathway owing to the lower barriers encountered, and theoretical calculations support this mechanism where the reaction proceeds via a complex [NCOO] and successive elimination of the O atom leading to an overall lowest energy barrier[75,77]. Moreover, literature suggests the NCO formed also may follow a mechanism similar to the roaming

mechanism[78], where the O abstracts a N from the complex leading to the products CO + NO. Interestingly, this may be one of the first suggested examples of roaming in neutral reactions, long before it was clearly identified in formaldehyde photodissociation.[79] The channel leading to CO+NO (2) is believed to proceed through a series of consecutive rearrangement of [NCOO] with a branching ratio of ~0.22 at 298 K[80] supporting roaming-like dynamics circumventing an otherwise high barrier from NCOO to CO + NO. The temperature dependent kinetics of the channel (2) has shown an increase in product branching ratio to 0.3 at 239 K, however there is no experimental evidence that this relationship remains accurate at much lower temperatures[80]. Over the impressive wide range of temperature the reaction has been studied experimentally the rate of reaction is nearly independent of the temperature from 4000 K down to 700 K, but the rate increases when the temperature is dropped below 700 K down to 13 K[2,3,74-76,81]. Moreover, there are few experiments that have studied the influence of the vibrational excitation of CN on the rate of reaction[3,41]. The findings from these studies show that above room temperature the rate of reaction of v=1 is faster than v=0 (ranging 20-40% faster)[3]. It is enticing to attribute faster reaction kinetics of the vibrationally excited counterpart to vibrational quenching in addition to reaction. However, on the basis of energy gap law and measured rates for both vibrationally excited and ground state rates at room temperature it is predicted the observed increase in rate could not arise simply from vibrational relaxation[41]. In addition, there is a lack of experiments conducted at lower temperatures for CN(v=1). Here we have

implemented UF-CRDS to measure the rate of reaction of CN(v=1) at temperatures much lower than room temperature (70 K and 24 K).

4.3.1 Results and Discussion

The ringdown ratio is measured for varying concentrations of O_2. As summarized by the SKaR technique, the background normalized ringdown ratio is calculated at both temperatures of 70 K and 24 K.

Table 4.1 Summary of reaction flow conditions and rates obtained for the reaction CN(v=1) +O_2.

Flow temperature/K	Gas	Flow density/ molecules cm^{-3}	Range of $[O_2]/10^{13}$ molecules cm^{-3}	No of measurements	Rate constant/ cm^3 molecule^{-1} s^{-1}
70	N_2	5.5×10^{16}	0.44-5.12	9	$(2.53 \pm 0.29) \times 10^{-11}$
24	Ne	4.5×10^{16}	0.18-2.12	7	$(1.33 \pm 0.26) \times 10^{-10}$

The derivative of the logarithm of ratio from equation 1.14 is plotted to extract time-dependent absorber kinetics. See figure 4.2 for the data plotted or 70 K and 24 K. The fitting time interval is chosen such that the hydrodynamic time is compatible with the reaction time. The excimer is fired at 20 μs after the ringdown event is triggered and the derivative of the logarithm of ratio suggests the time it takes the CN(v=1) to reach maximum is longer at 24 K than at 70 K. At 70 K this time is approximately 50 μs and for 24 K it is closer to 100 μs. We calculated the rate of this rise, and it does not depend on the concentration of O_2.
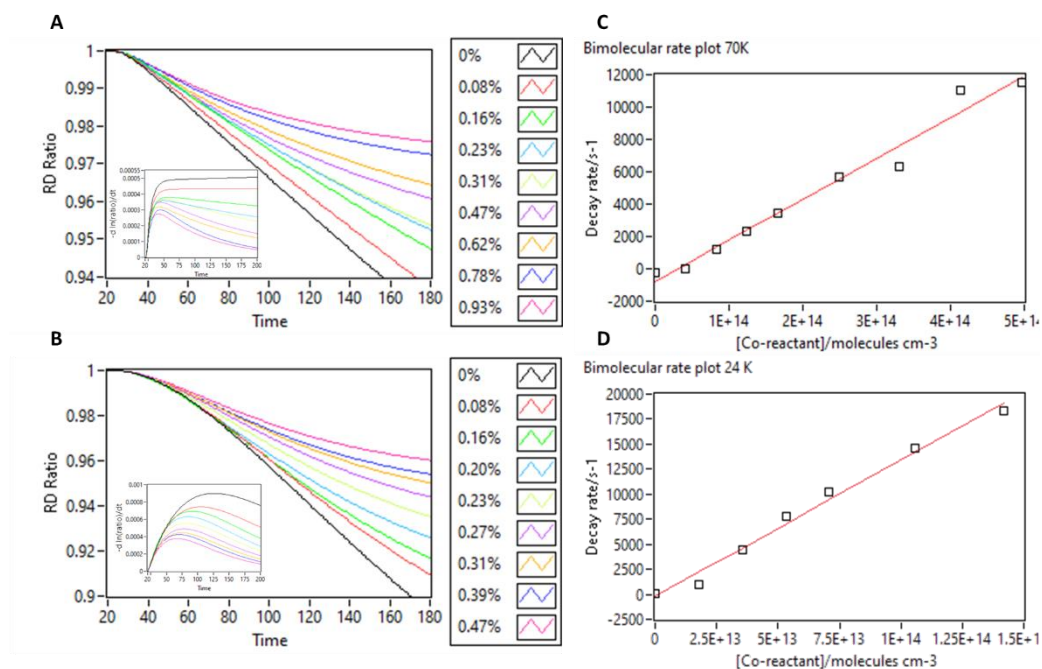
Figure 4.2 Background normalized ringdown ratio for CN(v=1) + O₂ reaction at 70 K (A) and 24 K(B). Inset: derivative of the logarithm of ratio with varying [O₂]. Bimolecular rate plots at 70 K (C) and 24 (D). The varying O₂ concentrations are given as a percentage of the total flow density 5.5x10¹⁶ molecule cm⁻³ and 4.5x10¹⁶ molecule cm⁻³ for 70 K and 24 K respectively.

The CN is probed approximately 15 cm from the nozzle exit and this allows roughly 170-200 μs of uniform flow conditions. Therefore, only up to a 180 us of the background normalized data is fitted to calculate the pseudo first order decay time. The measured bimolecular rate was 2.52×10^{-11} and 1.33×10^{-10} cm³ molecule⁻¹ s⁻¹ at 70 K and 24 K respectively.

The measured rates for the reaction is comapred with rates published by Sims et al. for CN(v=1) above room temperature[2](figure 4.3). At 24 K rate the measured agrees closely with the analogous (v=0) results from Sims and Smith (k = 1.33×10^{-10} cm³ mol⁻¹ s⁻¹), but the rate at 70 K is significantly lower than the v=0 rate (2.5 vs. 5.3×10^{-11} cm³ mol⁻¹ s⁻¹). Interestingly the rate at 70 K temperature

is very similar to the rates at higher temperatures that are largely independent of

the temperature. And this measured value is closely matched to the rate

calculated by Klippenstein et al using a variational statistical RRKM theoritical
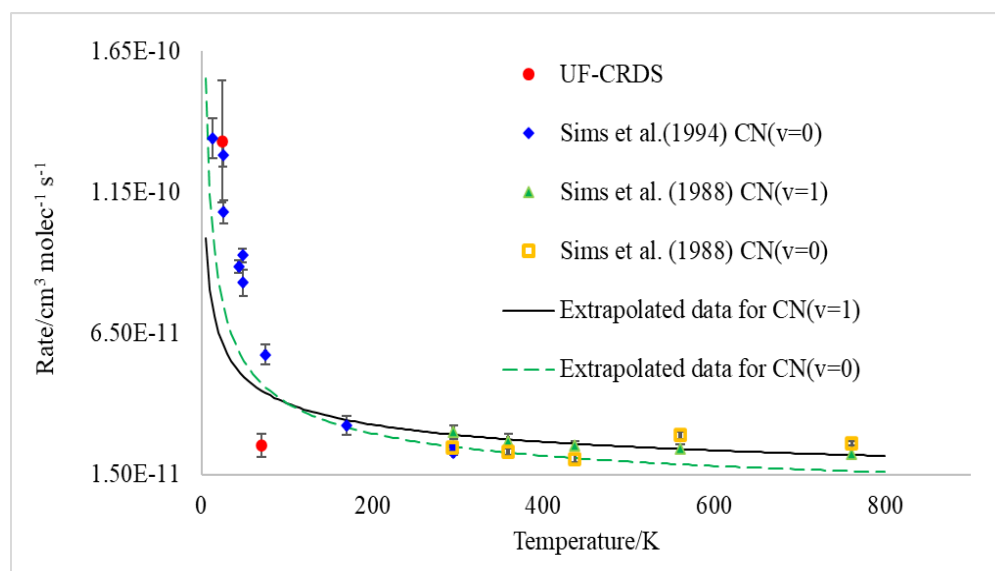
Figure 4.3 Comparison of the bimolecular rate measured with UF-CRDS for the reaction of CN with O_2 vs literature. (I. Sims et al., 1994)[2] (I. R. Sims & Smith, 1988)[3].

method[75].

4.4 Reaction of CN(v=1) with NO

The reaction of CN with NO is another example of an elementary neutral-neutral reaction. The fate of association of CN and NO can be given by the following.

$$CN(v) + NO \longrightarrow N_2 + CO \qquad (1)$$

$$CN(v) + NO + M \longrightarrow NOCN + M \qquad (2)$$

$$CN(v) + NO(v'=0) \longrightarrow CN(v-1) + NO(v'=1) \ (3)$$

LIF based investigations of the reactions of CN (v=0) and (v=1) at room temperature and above suggest the reaction of (v=1) with NO predominantly occurs via non-reactive vibrational relaxation process (3). This rate is much faster than either pathway leading to products though they are highly exothermic in nature (-635.8 kJ/mole and -204.3 kJ/mole for reaction (1) and (2) respectively)[82]. The increased rate due to vibrational relaxation can be explained by the energy gap law. Experimental results at low temperature and supporting theoretical calculations of CN+ NO suggest the reaction occurs dominantly via a channel where association yielding NCNO[82,83]. The vibrationally excited association, re-dissociates through non-reactive relaxation process[79]. This can be explained by the V-V transfer probabilities and the energy gaps between the vibrational states of the reactants (figure 4.3). The vibrational quenching is faster when the energy gap is smaller and the energy gap between the CN and NO for v=1 is 165 cm^{-1}. According to literature the rate of loss of CN above room temperature for v=1 is significantly faster in the presence of NO compared to pressure dependent rates of v=0[3,82]. However, the significant enhancement in

the rate of loss of CN (v=1) vs (v=0) can be attributed to formation and dissociation of [NCNO] complex though a barrierless analogous to the O_2 case above but without a reactive component. Here we report the rate of reaction of CN(v=1) with NO at temperatures 70 K and 24 K for the first time using UF-CRDS apparatus.
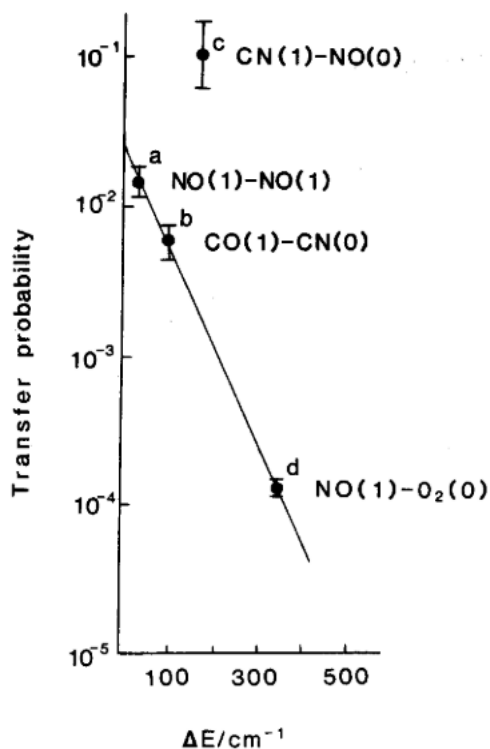
Figure 4.4 The plot of V-V transfer probabilities vs energy gap (from ref.[1])

4.4.1 Results and discussion

The pseudo first order rates were measured in the same way as explained in section 4.3.1. Analogous to the reaction with O_2, the time dependent change in concentration of CN reaches maximum faster at 70 K (in less than 50 μs) than

at 24 K. However, at 24 K at increased concentrations of NO, CN(v=1) reaches a peak faster (Figure 4.5). The measured rates at 70 K and 24 K are 9.95×10^{-11} and 1.93×10^{-10} cm^3 molecules^{-1} s^{-1} respectively. The reaction conditions are summarized in table 4.2. These measured rates follow the negative temperature dependence similar to what Sims I. et al. report[3]. Sims I. et al described the change of rate of reaction with temperature as following:

$$k = 7.6 \times 10^{-11}(T/298)^{-0.30}$$

The above relationship was derived for the temperature range of 296 to 761 K. When this relationship is extended to lower temperatures (Figure 4.6) the relationship does hold for the measured rates within the limit of uncertainties.

Table 4.2 Summary of reaction flow conditions and rates obtained for the reaction CN(v=1)+NO.

Flow temperature/K	Gas	Flow density/ molecules cm^{-3}	Range of [NO]/10^{14} molecules cm^{-3}	No of measurements	Rate constant/ cm^3 molecule^{-1} s^{-1}
70	N$_2$	5.5×10^{16}	0.2-2.4	7	$(9.95 \pm 0.94) \times 10^{-11}$
24	Ne	4.5×10^{16}	0.14-1.4	7	$(1.93 \pm 0.26) \times 10^{-10}$
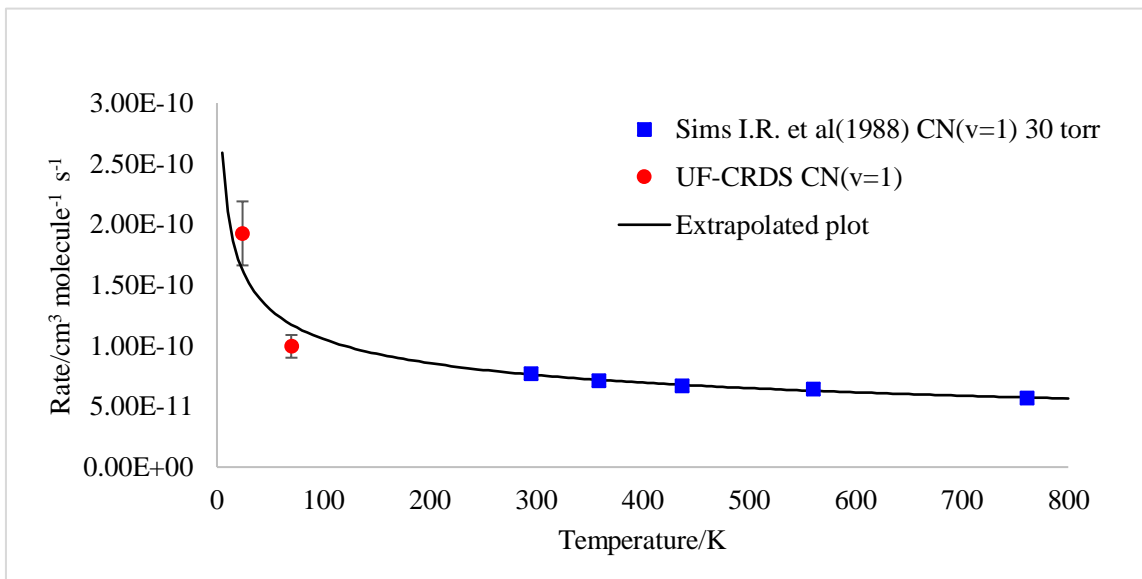
Figure 4.6 Comparison of the rates measured for the reaction CN(v=1) + NO using the current method (Red solid circle) and the literature (Blue solid square). The black solid line represents the extrapolated the rate from the expression derived for rate vs temperature by Sims I. et al[3].
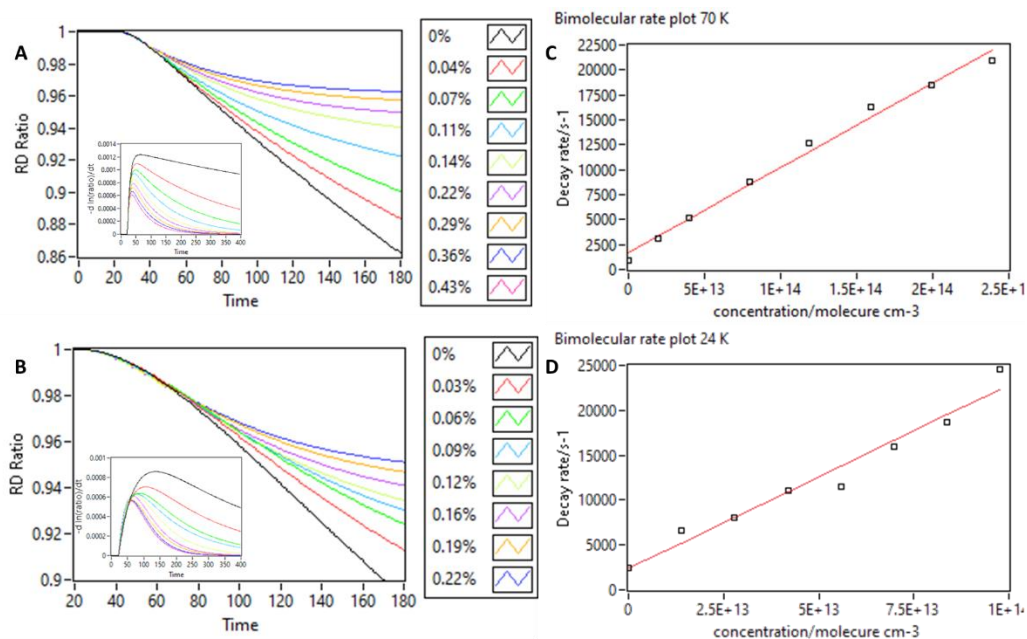
Figure 4.5 A, B Background normalized ringdown decay for varying [NO] at 70 K and 24 K respectively. Insets: the derivative of logarithm of the background normalized ringdown. The [NO] is given as a percentage of the flow density $5.5x10^{16}$ (70 K) and $4.5x10^{16}$ (24 K) molecules cm^{-3}. C,D the bimolecular rate plots at 70 K and 24 K respectively.

4.5 Conclusions

The current study reports rates of reaction of vibrationally excited CN(v=1) with O$_2$ and NO at low temperatures employing UF-CRDS. The rate of these reactions is comparable with the time interval at which a ringdown decay, thus we were able to successfully implement the SKaR method to measure these rates. The rates measured for both the reaction (with O$_2$) and the non-reactive relaxation (with NO) are quite fast at low temperature.

The measured rate for O$_2$ at 70 K is in great agreement with the rate calculated by Klippenstein et al using a variational statistical RRKM theoretical method[75] (UF-CRDS 2.53×10^{-11} cm^3 molecule^{-1} s^{-1} vs RRKM 2.7×10^{-11} cm^3 molecule^{-1} s^{-1}.). However, this rate is much slower than the rate reported by Sims et al for CN(v=0). In contrast, the rate measured at 24 K closely agrees with the reported for CN(v=0).

The rates measured for the non-reactive relaxation with NO does strongly follow the reported rates in literature.

CHAPTER 5

LOW TEMPERATURE KINETICS OF THE

REACTION OF CN(v=1) WITH BUTADIENE

ISOMERS

5.1 Introduction

The spectroscopic identification of nitrogen rich hydrocarbons in the interstellar medium, the atmosphere of Titan and meteoroids found on earth has propelled the interest in understanding reactions leading to nitrogen rich organic compounds[56,84-87]. Many astrochemical observations have accounts of nitrogen containing hydrocarbons such as complex amino acids[84], cyanopolyynes[88,89], ketenimine[90] and polycyclic aromatic hydrocarbon(PAH) such as 1-and 2-cyanonaphtaenes[91]. Moreover, identification and assigning he sources of unidentified infrared emission bands is task of great interest. These bands are attributed to emissions from PAH molecules. The advancement in spectroscopic methods coupled with CRESU[26,54,56,92] and theoretical approaches for the

Figure 5.2 Chemical structures of isomers of butadiene. A. 1,3-butadiene and B. 1,2-Butadiene.

reaction of CN provides considerable evidence that it is a major contributor leading to nitrogen rich compounds[56,92].

In this chapter we investigate reactions of vibrationally excited CN with isomers of butadiene (figure 5.1). Experimental and theoretical findings of reactions of ground state CN with isomers, 1,2- and 1,3-butadienes suggest the reaction enters through an entrance barrierless potential energy surface to form long lived C_5H_6N complexes leading to a range of possible products: [56,93]

$$CH_2{=}CH{-}CH{=}CH_2 + CN \longrightarrow CNCH{=}\underset{H}{C}{-}CH{=}CH_2 \qquad \Delta H = \text{-96 kJ mol}^{-1} \qquad (1)$$

$$CH_2{=}CH{-}CH{=}CH_2 + CN \longrightarrow \text{[pyridine ring]} + H \qquad \Delta H = \text{-195 kJ mol}^{-1} \qquad (2)$$

$$CH_2{=}C{=}CH{-}CH_3 + CN \longrightarrow CH_2{=}\underset{CN}{C}{-}CH{=}CH_2 + H \qquad \Delta H = \text{-141 kJ mol}^{-1} \qquad (3)$$

$$CH_2{=}C{=}CH{-}CH_3 + CN \longrightarrow \underset{CN}{\overset{}{CH_2}}{-}C{\equiv}CH + CH_3 \qquad \Delta H = \text{-109.6 kJ mol}^{-1} \qquad (4)$$

$$CH_2{=}C{=}CH{-}CH_3 + CN \longrightarrow H_2C{=}C{=}CHCN + CH_3 \quad \Delta H = \text{-125.52 kJ mol}^{-1} \qquad (5)$$
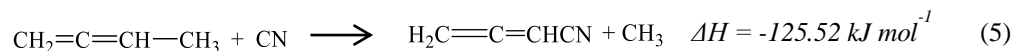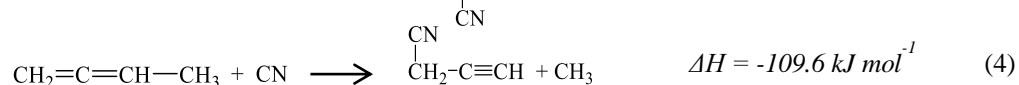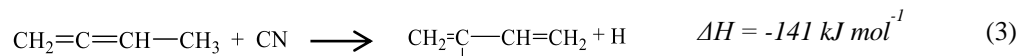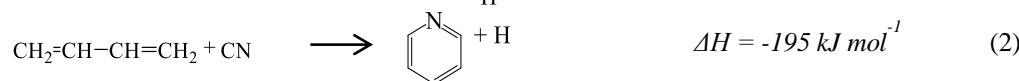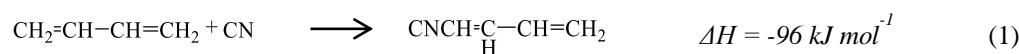
The reaction of 1,3-butadiene + CN can be either an addition or hydrogen abstraction (reaction 1 and 2). The results of crossed-molecular beam studies conducted at single collision conditions and supported by the electronic structure calculations suggests a nearly exclusive formation of thermodynamically less favorable product isomer 1-cyano-1,3-butadiene (1)[56]. The rates for the reaction with CN(v=0) has been reported for a wide range of temperatures ranging from 1200 K[54,94] to as low as 23 K[56]. The rates measured above room temperatures by both Butterfield et al.[54] and Gardez et al.[94] show a negative temperature

dependence while the experiments conducted at temperatures lower than room temperature (up to 24 K) using the CRESU apparatus by Morales et al. [56] has a positive temperature dependence though there is good agreement for the room temperature rate.

On the contrary, experimental measurement of the reaction of CN with 1,2-butadiene has not been reported to our knowledge. However, theoretical studies carried out by Jamal et al.[93] for the reaction between CN and 1,2-butadiene predicts three possible products and their branching ratios (reactions 3,4,and 5). The dominant product formed is 2-cyano-1,3-butadiene with almost 70-60 %, and the other products predicted are 1-cyano-prop-3-yne and cyanoallene.

Here we report measurement of rate of reaction of vibrationally excited CN(v=1) and both isomers 1,2- and 1,3-butadienes at 70 K using the UF-CRDS method. Further, we include theoretical calculations obtained by our collaborator Prof. Carlo Cavalotti of Milan Polytechnical University to determine the rates of reaction of CN+1,3-butadiene supplementary to the experimental measurements.

5.2 Experimental methods

The experiments were performed using the UF-CRDS apparatus. High purity ≥99.0% 1,2 and 1,3-butadiene are purchased from Sigma-Aldrich and used as is without any further purification. BrCN (Sigma Aldrich, reagent grade 97%) was used as the source of CN and prepared and used as described in Chapter 4. An

excimer operated at 248 nm was used as the photolysis laser (~75 mJ/pulse). The concentration of reactants and gas flow was controlled by flow controllers. The BrCN concentration is set at the lowest limit possible without compromising signal/noise to ensure pseudo first order conditions with respect to CN(v=1) and to reduce artifacts attributed to clustering. Measurements were made using two different Laval nozzles, one operated at 70 K (with N_2 flow gas) and the other operated at 24 K (with Ne as the flow gas). The loss of CN(v=1) is measured by tuning the DFB diode laser at 7070.240 cm^{-1} (j=5.5) and 7060.52 cm^{-1} (j=2.5) for the 70 K and 24 K measurements respectively. The CN was probed 20 cm from the exit of the nozzle which corresponds roughly to 200 us of hydrodynamic time. The ratio of the foreground and background ringdown is averaged for two time bins (400 us) and the decay rate is calculated by fitting the background normalized ringdown decay as described by the SKaR method.

5.3 Results and discussion

We report rate reaction of reaction of CN (v=1) with both 1,2-butadiene and 1,3-butadiene at 70 K flow conditions. Table 5.1 summarizes the reaction conditions and measured rates for the above reactions.

Table 5.1 Summary of reaction flow conditions and rates obtained for the reaction CN(v=1)+isomers of butadiene.

Isomer (temperature/K)	Gas	Flow density/ molecules cm^{-3}	Range of $[C_4H_6]/10^{13}$ molecules cm^{-3}	No of measurements	Rate constant/ cm^3 molecule^{-1} s^{-1}
1,2-butadiene(70)	N_2	5.5×10^{16}	0.81-6.52	7	3.06×10^{-10}
1,3-butadiene(70)	N_2	5.5×10^{16}	1.42-7.07	7	3.90×10^{-10}
1,3-butadiene(24)	Ne	4.5×10^{16}	0.59-7.15	7	2.61×10^{-10}

The measured rate for 1,3-butadiene is 3.90×10^{-10} and 2.61×10^{-10} cm^3 molecules^{-1} s^{-1} at 70 K and 24 K respectively. The rate measured for 1,3-butadiene at 70 K is in good agreement with the rate of reaction reported by Morales et al.[56] for loss of CN(v=0). However, the rate measured at 24 K is slower than the rate reported for the analogous species.

The rate measured for the reaction of CN(v=1) with 1,2-butadiene isomer at 70 K is 3.06×10^{-10} cm^3 molecules^{-1} s^{-1}. This is significantly slower than the corresponding rate for the 1,3 isomer. Although the conjugated isomer is more than 50 kJ/mol lower in energy than 1,2 butadiene, it has two accessible terminal sites for addition that can produce conjugated products. These terminal sites are
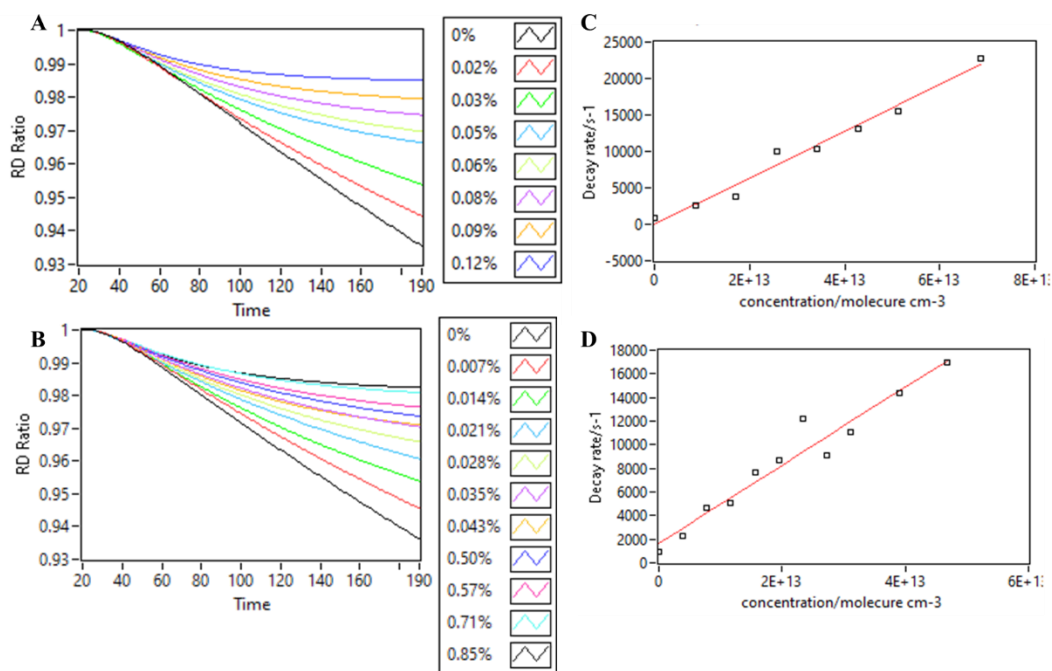
Figure 5.2 Background normalized ringdown decay for varying A. 1,2-butadiene and B. 1,3-butadiene. The [butadiene] is given as a percentage of the flow density 5.5×10^{16} (70 K) molecules cm^{-3}. C,D respective the bimolecular rate plots for pseudo first order rate vs 1,2- and 1,3-butadiene isomer density.

more reactive, and this can contribute to the long range attraction important at low temperature.

5.3.1 Theoretical modeling of the rate of reaction

Our collaborator Prof. Carlo Cavallotti, from Polytechnic University of Milan has performed theoretical calculations for the rate reaction of CN with the 1,3-butadiene isomer. For the calculations, contributions from central and terminal addition and abstraction are considered. Calculations for addition were performed using variable reaction coordinate transition state theory (VRC-TST)[95] simulations dividing the interaction potential energy surface in two parts: short range and long range interaction. Both short range and long range simulations were performed placing pivot points on the reactive carbon atoms, for both 1,3-butadiene and the CN radical. The two dynamic bottlenecks are indeed found for the reactive flux at long and short ranges. Up to about 1000K, the system is controlled by addition, after which abstraction starts gaining some relevance. At 70 K the reactive flux is controlled by long range interactions. The potential was computed at the CASPT2(11e,10o) level with aug-tz aug-qz basis set extrapolation to the complete basis set limit. However, a portion of the flux was leading to the formation of N-H bonded complexes between CN and 1,3-butadiene involving one H atom of 1,3-butadiene and the nitrogen atom of CN. To remove these fluxes from the total count, a fictitious repulsive potentials

between N and H[96] was added. The total rate constants were calculated for two recrossing coefficients, 0.9 (standard choice) and 0.8. (Figure 5.3). The experimental rates measured for 1,3-butadiene is in excellent agreement when the recrossing coefficient is set to 0.8. Further calculations for 1,2-butadiene are currently underway.

5.4 Conclusions

The reaction rates measured with UF-CRDS coupled with the SKaR method for the reaction of CN(v=1) with 1,3-butadiene at 70 K is in excellent agreement with the rate reported for the reaction with CN(v=0) by Morales et al. However, the there is a significant difference for that reported at 24 K. We also have reported for the first time the rate of reaction of CN(v=1) with 1,2-butadiene at 70 K and this rate is substantially lower compared to its 1,3-isomer. The
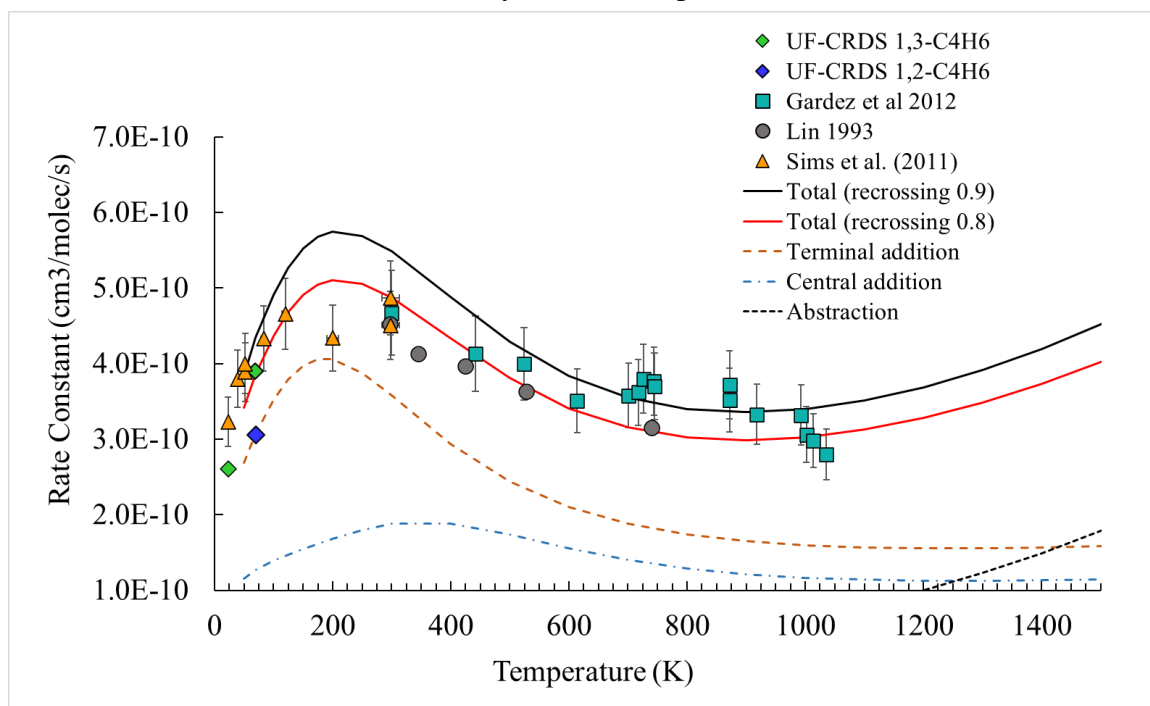
Figure 5.3 Comparison of experimental and theoretical temperature dependent rate of reaction of 1,3-butadiene+CN

72

theoretical calculations done using VRC-TST method provides excellent agreement to the experimental measurements of the 1,3-butadiene isomer and ongoing experiments and theory are evaluating the same for the 1,2-butadiene system.

REFERENCES

(1)   Li, X.; Sayah, N.; Jackson, W. M. A large vibrational enhancement in the reaction of CN (v '= 1, 2)+ NO. *The Journal of chemical physics* **1985,** *83* (2), 616.

(2)   Sims, I.; Queffelec, J. L.; Defrance, A.; Rebrion-Rowe, C.; Travers, D.; Bocherel, P.; Rowe, B.; Smith, I. W. Ultralow temperature kinetics of neutral–neutral reactions. The technique and results for the reactions CN+ O2 down to 13 K and CN+ NH3 down to 25 K. *The Journal of chemical physics* **1994,** *100* (6), 4229.

(3)   Sims, I. R.; Smith, I. W. Pulsed laser photolysis–laser-induced fluorescence measurements on the kinetics of CN (v= 0) and CN (v= 1) with O 2, NH 3 and NO between 294 and 761 K. *Journal of the Chemical Society, Faraday Transactions 2: Molecular and Chemical Physics* **1988,** *84* (5), 527.

(4)   Rowe, B.; Dupeyrat, G.; Marquette, J.; Gaucherel, P. Study of the reactions N+ 2+ 2N2→ N+ 4+ N2 and O+ 2+ 2O2→ O+ 4+ O2 from 20 to 160 K by the CRESU technique. *The Journal of chemical physics* **1984,** *80* (10), 4915.

(5)   Abeysekera, C.; Zack, L. N.; Park, G. B.; Joalland, B.; Oldham, J. M.; Prozument, K.; Ariyasingha, N. M.; Sims, I. R.; Field, R. W.; Suits, A. G. A chirped-pulse Fourier-transform microwave/pulsed uniform flow spectrometer. II. Performance and applications for reaction dynamics. *The Journal of chemical physics* **2014,** *141* (21), 214203.

(6)   Oldham, J. M.; Abeysekera, C.; Joalland, B.; Zack, L. N.; Prozument, K.; Sims, I. R.; Park, G. B.; Field, R. W.; Suits, A. G. A chirped-pulse Fourier-transform microwave/pulsed uniform flow spectrometer. I. The low-temperature flow system. *The Journal of chemical physics* **2014,** *141* (15), 154202.

(7)   O'Keefe, A.; Deacon, D. A. Cavity ring-down optical spectrometer for absorption measurements using pulsed laser sources. *Review of Scientific Instruments* **1988,** *59* (12), 2544.

(8)   Romanini, D.; Kachanov, A.; Sadeghi, N.; Stoeckel, F. CW cavity ring down spectroscopy. *Chemical Physics Letters* **1997,** *264* (3-4), 316.

(9)   Brown, S. S.; Ravishankara, A.; Stark, H. Simultaneous kinetics and ring-down: rate coefficients from single cavity loss temporal profiles. *The Journal of Physical Chemistry A* **2000,** *104* (30), 7044.

(10)   Van Helden, J.; Peverall, R.; Ritchie, G.; Berden, G.; Engeln, R. *Cavity enhanced techniques using continuous wave lasers*; Wiley-Blackwell West Sussex, UK, 2009.

(11)   Yariv, A.; Yeh, P. *Photonics: optical electronics in modern communications*; Oxford university press, 2007.

(12)   Rowe, B.; Dupeyrat, G.; Marquette, J.; Smith, D.; Adams, N.; Ferguson, E. The reaction O+ 2+ CH4→ CH3O+ 2+ H studied from 20 to 560 K in a supersonic jet and in a SIFT. *The Journal of chemical physics* **1984,** *80* (1), 241.

(13)   Rowe, B.; Marquette, J. CRESU studies of ion/molecule reactions. *International journal of mass spectrometry and ion processes* **1987,** *80*, 239.

(14)   Sims, I.; Queffelec, J.; Defrance, A.; Rebrion-Rowe, C.; Travers, D.; Rowe, B.; Smith, I. Ultra-low temperature kinetics of neutral–neutral reactions: The reaction CN+ O2 down to 26 K. *The Journal of chemical physics* **1992,** *97* (11), 8798.

(15)   Sims, I. R.; Smith, I. W. Gas-phase reactions and energy transfer at very low temperatures. *Annual review of physical chemistry* **1995,** *46* (1), 109.

(16)   Moger, W.; Ramsay, D. "Supersonic axisymmetric nozzle design by mass flow techniques utilizing a digital computer," ARNOLD ENGINEERING DEVELOPMENT CENTER ARNOLD AFB TN, 1964.

(17)   Atkinson, D. B.; Smith, M. A. Design and characterization of pulsed uniform supersonic expansions for chemical applications. *Review of scientific instruments* **1995,** *66* (9), 4434.

(18)   Canosa, A.; Ocaña, A.; Antinolo, M.; Ballesteros, B.; Jiménez, E.; Albaladejo, J. Design and testing of temperature tunable de Laval nozzles for applications in gas-phase reaction kinetics. *Experiments in fluids* **2016,** *57* (9), 152.

(19)   Durif, O. Design of de Laval nozzles for gas-phase molecular studies in uniform supersonic flow. *Physics of Fluids* **2022,** *34* (1), 013605.

(20)   Lee, P. A.; Anderson, J. D. *Modern Compressible Flow, with Historical Perspective*; McGraw-Hill Science, Engineering & Mathematics, 1982.

(21)   Fournier, M.; Le Picard, S. D.; Sims, I. R. Low-temperature chemistry in uniform supersonic flows. **2017**.

(22)   Lee, S.; Hoobler, R. J.; Leone, S. R. A pulsed Laval nozzle apparatus with laser ionization mass spectroscopy for direct measurements of rate coefficients at low temperatures with condensable gases. *Review of Scientific Instruments* **2000,** *71* (4), 1816.

(23)   Taylor, S. E.; Goddard, A.; Blitz, M. A.; Cleary, P. A.; Heard, D. E. Pulsed Laval nozzle study of the kinetics of OH with unsaturated hydrocarbons at very low temperatures. *Physical Chemistry Chemical Physics* **2008,** *10* (3), 422.

(24)   Suas-David, N.; Thawoos, S.; Suits, A. G. A uniform flow–cavity ring-down spectrometer (UF-CRDS): A new setup for spectroscopy and kinetics at low temperature. *The Journal of Chemical Physics* **2019,** *151* (24), 244202.

(25)   Abeysekera, C.; Joalland, B.; Shi, Y.; Kamasah, A.; Oldham, J. M.; Suits, A. G. Note: A short-pulse high-intensity molecular beam valve

based on a piezoelectric stack actuator. *Review of Scientific Instruments* **2014,** *85* (11), 116107.

(26)   Broderick, B. M.; Suas-David, N.; Dias, N.; Suits, A. G. Isomer-specific detection in the UV photodissociation of the propargyl radical by chirped-pulse mm-wave spectroscopy in a pulsed quasi-uniform flow. *Physical Chemistry Chemical Physics* **2018**.

(27)   Hippler, M.; Quack, M. Cw cavity ring-down infrared absorption spectroscopy in pulsed supersonic jets: nitrous oxide and methane. *Chemical physics letters* **1999,** *314* (3), 273.

(28)   Birza, P.; Motylewski, T.; Khoroshev, D.; Chirokolava, A.; Linnartz, H.; Maier, J. Cw cavity ring down spectroscopy in a pulsed planar plasma expansion. *Chemical Physics* **2002,** *283* (1-2), 119.

(29)   Motylewski, T.; Linnartz, H. Cavity ring down spectroscopy on radicals in a supersonic slit nozzle discharge. *Review of scientific instruments* **1999,** *70* (2), 1305.

(30)   Verbraak, H.; Ngai, A.; Persijn, S.; Harren, F.; Linnartz, H. Mid-infrared continuous wave cavity ring down spectroscopy of molecular ions using an optical parametric oscillator. *Chemical physics letters* **2007,** *442* (1-3), 145.

(31)   Suas-David, N.; Kulkarni, V.; Benidar, A.; Kassi, S.; Georges, R. Line shape in a free-jet hypersonic expansion investigated by cavity ring-down spectroscopy and computational fluid dynamics. *Chemical Physics Letters* **2016,** *659*, 209.

(32)   North, S. W.; Zheng, X. S.; Fei, R.; Hall, G. E. Line shape analysis of Doppler broadened frequency-modulated line spectra. *The Journal of chemical physics* **1996,** *104* (6), 2129.

(33)   Zare, R. N.; Herschbach, D. R. Doppler line shape of atomic fluorescence excited by molecular photodissociation. *Proceedings of the IEEE* **1963,** *51* (1), 173.

(34)   Romanini, D.; Dupré, P.; Jost, R. Non-linear effects by continuous wave cavity ringdown spectroscopy in jet-cooled NO2. *Vibrational spectroscopy* **1999,** *19* (1), 93.

(35)   Hause, M. L.; Hall, G. E.; Sears, T. J. Sub-Doppler laser absorption spectroscopy of the A2Πi− X2Σ+(1, 0) band of CN: Measurement of the 14N hyperfine parameters in A2Π CN. *Journal of Molecular Spectroscopy* **2009,** *253* (2), 122.

(36)   Brooke, J. S.; Ram, R. S.; Western, C. M.; Li, G.; Schwenke, D. W.; Bernath, P. F. Einstein A Coefficients and Oscillator Strengths for the A 2Π-X 2Σ+(Red) and B2Σ+-X2Σ+(Violet) Systems and Rovibrational Transitions in the X 2Σ+ State of CN. *The Astrophysical Journal Supplement Series* **2014,** *210* (2), 23.

(37)   Russell, J. A.; McLaren, I. A.; Jackson, W. M.; Halpern, J. B. Photolysis of cyanogen bromide between 193 and 266 nm. *Journal of Physical Chemistry* **1987,** *91* (12), 3248.

(38)   Felps, W.; Rupnik, K.; McGlynn, S. Electronic spectroscopy of the cyanogen halides. *Journal of physical chemistry* **1991,** *95* (2), 639.

(39)   Fisher, W.; Eng, R.; Carrington, T.; Dugan, C.; Filseth, S.; Sadowski, C. Photodissociation of BrCN and ICN in the a continuum: Vibrational and rotational distributions of CN (X 2Σ+). *Chemical physics* **1984,** *89* (3), 457.

(40)   Huang, C.; Li, W.; Silva, R.; Suits, A. G. DC slice ion imaging of the ultraviolet photodissociation of BrCN. *Chemical physics letters* **2006,** *426* (4-6), 242.

(41)   Li, X.; Sayah, N.; Jackson, W. M. Laser measurements of the effects of vibrational energy on the reactions of CN. *The Journal of chemical physics* **1984,** *81* (2), 833.

(42)   Saidani, G.; Kalugina, Y.; Gardez, A.; Biennier, L.; Georges, R.; Lique, F. High temperature reaction kinetics of CN (v= 0) with C2H4 and C2H6 and vibrational relaxation of CN (v= 1) with Ar and He. *The Journal of chemical physics* **2013,** *138* (12), 124308.

(43)   Mertens, L. A.; Labiad, H.; Denis-Alpizar, O.; Fournier, M.; Carty, D.; Le Picard, S. D.; Stoecklin, T.; Sims, I. R. Rotational energy transfer in collisions between CO and Ar at temperatures from 293 to 30 K. *Chemical Physics Letters* **2017,** *683*, 521.

(44)   Hay, S.; Shokoohi, F.; Callister, S.; Wittig, C. Collisional metastability of high rotational states of CN (X2Σ+,= 0). *Chemical physics letters* **1985,** *118* (1), 6.

(45)   Jiménez, E.; Ballesteros, B.; Canosa, A.; Townsend, T.; Maigler, F.; Napal, V.; Rowe, B.; Albaladejo, J. Development of a pulsed uniform supersonic gas expansion system based on an aerodynamic chopper for gas phase reaction kinetic studies at ultra-low temperatures. *Review of Scientific Instruments* **2015,** *86* (4), 045108.

(46)   Lichtin, D.; Lin, M. Kinetics of CN radical reactions with selected molecules at room temperature. *Chemical physics* **1985,** *96* (3), 473.

(47)   Zabarnick, S.; Lin, M. Kinetics of CN (X 2Σ+) radical reactions with HCN, BrCN and CH3CN. *Chemical Physics* **1989,** *134* (1), 185.

(48)   Caballero, J.; Jackson, W.; Li, X.; Sayah, N. Laser measurements of the quenching and reaction of CN radicals with BrCN and ClCN. *Journal of Photochemistry and Photobiology A: Chemistry* **1989,** *47* (1), 41.

(49)   Gannon, K. L.; Glowacki, D. R.; Blitz, M. A.; Hughes, K. J.; Pilling, M. J.; Seakins, P. W. H Atom Yields from the Reactions of CN Radicals with C2H2, C2H4, C3H6, trans-2-C4H8, and iso-C4H8. *The Journal of Physical Chemistry A* **2007,** *111* (29), 6679.

(50)   Morales, S. B.; Le Picard, S. D.; Canosa, A.; Sims, I. R. Experimental measurements of low temperature rate coefficients for neutral–neutral reactions of interest for atmospheric chemistry of Titan, Pluto and Triton: reactions of the CN radical. *Faraday discussions* **2010,** *147*, 155.

(51)   Sims, I. R.; Queffelec, J.-L.; Travers, D.; Rowe, B. R.; Herbert, L. B.; Karthäuser, J.; Smith, I. W. Rate constants for the reactions of CN with hydrocarbons at low and ultra-low temperatures. *Chemical Physics Letters* **1993,** *211* (4-5), 461.

(52)   Trevitt, A. J.; Goulay, F.; Taatjes, C. A.; Osborn, D. L.; Leone, S. R. Reactions of the CN radical with benzene and toluene: Product detection and low-temperature kinetics. *The Journal of Physical Chemistry A* **2010,** *114* (4), 1749.

(53)   Stoecklin, T.; Dateo, C.; Clary, D. Rate constant calculations on fast diatom–diatom reactions. *Journal of the Chemical Society, Faraday Transactions* **1991,** *87* (11), 1667.

(54)   Butterfield, M. T.; Yu, T.; Lin, M. Kinetics of CN reactions with allene, butadiene, propylene and acrylonitrile. *Chemical physics* **1993,** *169* (1), 129.

(55)   Carty, D.; Le Page, V.; Sims, I. R.; Smith, I. W. Low temperature rate coefficients for the reactions of CN and C2H radicals with allene (CH2☐C☐CH2) and methyl acetylene (CH3C☐CH). *Chemical Physics Letters* **2001,** *344* (3-4), 310.

(56)   Morales, S. B.; Bennett, C. J.; Le Picard, S. D.; Canosa, A.; Sims, I. R.; Sun, B.; Chen, P.; Chang, A. H.; Kislov, V. V.; Mebel, A. M.et al. A Crossed Molecular Beam, Low-Temperature Kinetics, and Theoretical Investigation of the Reaction of the Cyano Radical (CN) with 1, 3-Butadiene (C4H6). A Route to Complex Nitrogen-Bearing Molecules in Low-Temperature Extraterrestrial Environments. *The Astrophysical Journal* **2011,** *742* (1), 26.

(57)   Bullock, G.; Cooper, R. Reactions of cyanogen radicals. Part 2.— Reactions with (CN) 2 and O 2. *Journal of the Chemical Society, Faraday Transactions 1: Physical Chemistry in Condensed Phases* **1972,** *68*, 2175.

(58)   Schacke, H.; Schmatjko, K.; Wolfrum, J. Reaktionen von Molekülen in definierten Schwingungszuständen (I) Die Reaktionen CN (v ")+ O und CN (v")+ O2. *Ber. Bunsenges. Phys. Chem.* **1973,** *77* (4), 248.

(59)   Whyte, A.; Phillips, L. Rate of reaction of N with CN (υ= 0, 1). *Chemical physics letters* **1983,** *98* (6), 590.

(60)   Atakan, B.; Jacobs, A.; Wahl, M.; Weller, R.; Wolfrum, J. Kinetic studies of the gas-phase reactions of CN with O2 and H2 from 294 to 1000 K. *Chemical Physics Letters* **1989,** *154* (5), 449.

(61)   Schacke, H.; Wagner, H. G.; Wolfrum, J. Reaktionen von Molekülen in definierten Schwingungszuständen (IV). Reaktionen schwingungsangeregter Cyan-Radikale mit Wasserstoff und einfachen Kohlenwasserstoffen. *Ber. Bunsenges. Phys. Chem.* **1977,** *81* (7), 670.

(62)   De Juan, J.; Smith, I. W.; Veyret, B. Kinetics of CN (v= 0) and CN (v= 1) with H2 HCl and HBr. *Chemical physics letters* **1986,** *132* (2), 108.

(63)   Sims, I. R.; Smith, I. W. Rate constants for the reactions CN (υ= 0), CN (υ= 1)+ H2, D2→ HCN, DCN+ H, D between 295 and 768 K, and comparisons with transition state theory calculations. *Chemical physics letters* **1988,** *149* (5-6), 565.

(64)   Bullock, G.; Cooper, R. Reactions of cyanogen radicals. Part 3.— Arrhenius parameters for reactions with alkanes. *Journal of the*

Chemical Society, Faraday Transactions 1: Physical Chemistry in Condensed Phases **1972,** *68*, 2185.

(65)   Herbert, L.; Smith, I. W.; Spencer-smith, R. D. Rate constants for the elementary reactions between CN radicals and CH4, C2H6, C2H4, C3H6, and C2H2 in the range: 295⩽ T/K⩽ 700. *International journal of chemical kinetics* **1992,** *24* (9), 791.

(66)   Smith, I. W. Vibrational adiabaticity in chemical reactions. *Accounts of Chemical Research* **1990,** *23* (4), 101.

(67)   Sayah, N.; Li, X.; Caballero, J.; Jackson, W. M. Laser induced fluorescence studies of CN reactions with alkanes, alkenes and substituted aliphatic species. *Journal of Photochemistry and Photobiology A: Chemistry* **1988,** *45* (2), 177.

(68)   Brownsword, R. A.; Canosa, A.; Rowe, B. R.; Sims, I. R.; Smith, I. W.; Stewart, D. W.; Symonds, A. C.; Travers, D. Kinetics over a wide range of temperature (13–744 K): rate constants for the reactions of CH (*v*= 0) with H 2 and D 2 and for the removal of CH (*v*= 1) by H 2 and D 2. *The Journal of chemical physics* **1997,** *106* (18), 7662.

(69)   Cernicharo, J.; Agúndez, M.; Kahane, C.; Guélin, M.; Goicoechea, J.; Marcelino, N.; De Beck, E.; Decin, L. Probing the dust formation region in IRC+ 10216 with the high vibrational states of hydrogen cyanide. *Astronomy & Astrophysics* **2011,** *529*, L3.

(70)   O'Halloran, M. A.; Joswig, H.; Zare, R. N. Alignment of CN from 248 nm photolysis of ICN: A new model of the Ã continuum dissociation dynamics. *The Journal of chemical physics* **1987,** *87* (1), 303.

(71)   Lam, L.; Dugan, C.; Sadowski, C. The gas phase reactions of CN and NO. *The Journal of Chemical Physics* **1978,** *69* (6), 2877.

(72)   Kanda, K.; Katsumata, S.; Nagata, T.; Ozaki, Y.; Kondow, T.; Kuchitsu, K.; Hiraya, A.; Shobatake, K. Photodissociation of BrCN in the vacuum ultraviolet region. *Chemical physics* **1993,** *175* (2-3), 399.

(73)   Clary, D. C.; Stoecklin, T. S.; Wickham, A. G. Rate constants for chemical reactions of radicals at low temperatures. *Journal of the Chemical Society, Faraday Transactions* **1993,** *89* (13), 2185.

(74)   Durant Jr, J.; Tully, F. P. Kinetic study of the reaction between CN AND O2 from 295 to 710 K. *Chemical physics letters* **1989,** *154* (6), 568.

(75)   Klippenstein, S. J.; Kim, Y. W. Variational statistical study of the CN+ O2 reaction employing ab initio determined properties for the transition state. *The Journal of chemical physics* **1993,** *99* (8), 5790.

(76)   Balla, R. J.; Casleton, K. H. Kinetic study of the reactions of cyanyl radical with oxygen and carbon dioxide from 292 to 1500 K using high-temperature photochemistry. *The Journal of Physical Chemistry* **1991,** *95* (6), 2344.

(77)   Qu, Z.-w.; Zhu, H.; Li, Z.-s.; Zhang, X.-k.; Zhang, Q.-y. Theoretical study on the mechanism of the reaction between CN and O2. *Chemical physics letters* **2002,** *353* (3-4), 304.

(78) Mohammad, F.; Morris, V. R.; Fink, W. H.; Jackson, W. M. On the mechanism and branching ratio of the CN+ O2→ CO+ NO reaction channel using transient IR emission spectroscopy. *Journal of physical chemistry* **1993,** *97* (45), 11590.

(79) Qian, C.; Noble, M.; Nadler, I.; Reisler, H.; Wittig, C. NCNO→ CN+ NO: Complete NO (E, V, R) and CN (V, R) nascent population distributions from well-characterized monoenergetic unimolecular reactions. *The Journal of chemical physics* **1985,** *83* (11), 5573.

(80) Rim, K. T.; Hershberger, J. F. Temperature dependence of the product branching ratio of the CN+ O2 reaction. *The Journal of Physical Chemistry A* **1999,** *103* (19), 3721.

(81) Smith, I. W. The temperature-dependence of elementary reaction rates: beyond Arrhenius. *Chemical Society Reviews* **2008,** *37* (4), 812.

(82) Sims, I. R.; Smith, I. W. M. Pressure and temperature dependence of the rate of reaction between CN radicals and NO over the range 99⩽ T/K⩽ 450. *Journal of the Chemical Society, Faraday Transactions* **1993,** *89* (1), 1.

(83) Klippenstein, S. J.; Yang, D.; Yu, T.; Kristyan, S.; Lin, M.; Robertson, S. A theoretical and experimental study of the CN+ NO association reaction. *The Journal of Physical Chemistry A* **1998,** *102* (35), 6973.

(84) Elsila, J. E.; Dworkin, J. P.; Bernstein, M. P.; Martin, M. P.; Sandford, S. A. Mechanisms of amino acid formation in interstellar ice analogs. *The Astrophysical Journal* **2007,** *660* (1), 911.

(85) Loison, J.; Hébrard, E.; Dobrijevic, M.; Hickson, K.; Caralp, F.; Hue, V.; Gronoff, G.; Venot, O.; Bénilan, Y. The neutral photochemistry of nitriles, amines and imines in the atmosphere of Titan. *Icarus* **2015,** *247*, 218.

(86) Bullock, G.; Cooper, R. Reactions of cyanogen radicals with hydrocarbons. *Transactions of the Faraday Society* **1971,** *67*, 3258.

(87) Belloche, A.; Garrod, R.; Müller, H.; Menten, K.; Comito, C.; Schilke, P. Increased complexity in interstellar chemistry: detection and chemical modeling of ethyl formate and n-propyl cyanide in Sagittarius B2 (N). *Astronomy & Astrophysics* **2009,** *499* (1), 215.

(88) Paubert, G.; Gautier, D.; Courtin, R. The millimeter spectrum of Titan: Detectability of HCN, HC3N, and CH3CN and the CO abundance. *Icarus* **1984,** *60* (3), 599.

(89) Arnau, A.; Tunon, I.; Silla, E.; Andres, J. HCnN: The largest molecules in the interstellar medium. *Journal of Chemical Education* **1990,** *67* (11), 905.

(90) Lovas, F. J.; Hollis, J.; Remijan, A. J.; Jewell, P. Detection of ketenimine (CH2CNH) in Sagittarius B2 (N) hot cores. *The Astrophysical Journal* **2006,** *645* (2), L137.

(91) McGuire, B. A.; Loomis, R. A.; Burkhardt, A. M.; Lee, K. L. K.; Shingledecker, C. N.; Charnley, S. B.; Cooke, I. R.; Cordiner, M. A.; Herbst, E.; Kalenskii, S. Detection of two interstellar polycyclic

aromatic hydrocarbons via spectral matched filtering. *Science* **2021,** *371* (6535), 1265.

(92)   Rowe, B.; Rowe, C. R.; Canosa, A. Symposium-International Astronomical Union, 2000; p 237.

(93)   Jamal, A.; Mebel, A. M. Theoretical investigation of the mechanism and product branching ratios of the reactions of cyano radical with 1- and 2-butyne and 1, 2-butadiene. *The Journal of Physical Chemistry A* **2013,** *117* (4), 741.

(94)   Gardez, A.; Saidani, G.; Biennier, L.; Georges, R.; Hugo, E.; Chandrasekaran, V.; Roussel, V.; Rowe, B.; Reddy, K.; Arunan, E. High-temperature kinetics of the reaction between CN and hydrocarbons using a novel high-enthalpy flow tube. *International Journal of Chemical Kinetics* **2012,** *44* (11), 753.

(95)   Klippenstein, S. J.; Cavallotti, C. In *Computer Aided Chemical Engineering*; Elsevier, 2019; Vol. 45.

(96)   Puzzarini, C.; Salta, Z.; Tasinato, N.; Lupi, J.; Cavallotti, C.; Barone, V. A twist on the reaction of the CN radical with methylamine in the interstellar medium: new hints from a state-of-the-art quantum-chemical study. *Monthly Notices of the Royal Astronomical Society* **2020,** *496* (4), 4298.

VITA

Shameemah Thawoos was born in central Sri Lanka, obtained a Bachelor of Science in Chemistry from University of Peradeniya in 2012. Moved to the United States to pursuit her Ph.D at Wayne State University, Detroit MI in August 2014. Completed graduate course work at Wayne State University and conducted the research under the supervision of Professor. Sarah Trimpin. Upon moving to University of Missouri, Columbia in May 2016 to continued to work on completing her Ph.D under the supervision of Professor Arthur G Suits. During her time at Suits group, Shameemah worked on a new experiment, which involved combining cavity ringdown spectroscopy with a pulsed Laval flow to study gas phase reaction kinetics and dynamics.